Collision Chronology Along the İzmir-Ankara-Erzincan Suture Zone: Insights From the Sarıcakaya Basin, Western Anatolia

M. A Mueller, A. Licht, C. Campbell, F. Ocakoğlu, M. H Taylor, L. Burch, T. Ugrai, M. Kaya, B. Kurtoğlu, P. M C Coster, et al.

Tectonics

RESEARCH ARTICLE
10.1029/2019TC005683

Special Section:
Tethyan dynamics: from rifting to collision

Collision Chronology Along the İzmir-Ankara-Erzincan Suture Zone: Insights From the Sarıcakaya Basin, Western Anatolia

M. A. Mueller[1], A. Licht[1], C. Campbell[2], F. Ocakoğlu[3], M. H. Taylor[2], L. Burch[1], T. Ugrai[4], M. Kaya[5], B. Kurtoğlu[6,7], P. M. C. Coster[8], G. Métais[9], and K. C. Beard[8,10]

[1]Department of Earth and Space Sciences, University of Washington, Seattle, WA, USA, [2]Department of Geology, University of Kansas, Lawrence, KS, USA, [3]Department of Geological Engineering, Eskişehir Osmangazi University, Eskişehir, Turkey, [4]School of Oceanography, University of Washington, Seattle, WA, USA, [5]Institute of Geosciences, Universitat Potsdam, Potsdam, Germany, [6]Department of Geological Engineering, Middle East Technical University, Ankara, Turkey, [7]Department of Geological Sciences, University of Missouri, Columbia, MO, USA, [8]Biodiversity Institute, University of Kansas, Lawrence, KS, USA, [9]Centre de recherche sur la paléobiodiversité et les paléoenvironnements, Muséum National d'Histoire Naturelle, Paris, France, [10]Department of Ecology and Evolutionary Biology, University of Kansas, Lawrence, KS, USA

Abstract Debate persists concerning the timing and geodynamics of intercontinental collision, style of syncollisional deformation, and development of topography and fold-and-thrust belts along the >1,700-km-long İzmir-Ankara-Erzincan suture zone (İAESZ) in Turkey. Resolving this debate is a necessary precursor to evaluating the integrity of convergent margin models and kinematic, topographic, and biogeographic reconstructions of the Mediterranean domain. Geodynamic models argue either for a synchronous or diachronous collision during either the Late Cretaceous and/or Eocene, followed by Eocene slab breakoff and postcollisional magmatism.

We investigate the collision chronology in western Anatolia as recorded in the sedimentary archives of the 90-km-long Sarıcakaya Basin perched at shallow structural levels along the İAESZ. Based on new zircon U-Pb geochronology and depositional environment and sedimentary provenance results, we demonstrate that the Sarıcakaya Basin is an Eocene sedimentary basin with sediment sourced from both the İAESZ and Söğüt Thrust fault to the south and north, respectively, and formed primarily by flexural loading from north-south shortening along the syncollisional Söğüt Thrust. Our results refine the timing of collision between the Anatolides and Pontide terranes in western Anatolia to Maastrichtian-Middle Paleocene and Early Eocene crustal shortening and basin formation. Furthermore, we demonstrate contemporaneous collision, deformation, and magmatism across the İAESZ, supporting synchronous collision models. We show that regional postcollisional magmatism can be explained by renewed underthrusting instead of slab breakoff. This new İAESZ chronology provides additional constraints for kinematic, geodynamic, and biogeographic reconstructions of the Mediterranean domain.

Plain Language Summary The timeline of continent-continent collisions and the creation of topography, volcanic activity, and thrust faults in Anatolia (Turkey) are highly debated. Continent-continent collision occurs when oceanic crust between two continental plates has been entirely consumed back into the Earth's interior along a subduction zone. Previous work in western Anatolia suggests that 66–60 million years ago continent-continent collision was followed by catastrophic rupturing of the sinking oceanic crust, a process known as slab breakoff. Numerical models and field observations demonstrate that slab breakoff is followed by rebound and surface uplift of the overriding plate producing local extension and interrupting sedimentation. By studying a syncollisional sedimentary basin, we determined the sedimentary infill is 52–48 million years old and sourced from both continents, indicating collision must have occurred prior to 52 million years ago. This timing validates previous predictions of synchronous collision across western and central Turkey. Furthermore, the timing of basin infill directly overlaps with the timing of proposed slab breakoff. Our observations and data contradict predictions of the slab breakoff model making breakoff an unlikely candidate. Instead, we propose continued shortening and collision as the cause for the co-occurrence of sedimentary basin formation, deformation, and volcanism observed throughout western Turkey.

Key Points:
- The Sarıcakaya Basin is an Eocene sedimentary basin formed by flexural loading from the syncollisional Sogut Thrust fault
- Sarıcakaya Basin magmatism and deformation chronology are similar to central Anatolia, supporting synchronous collision across Anatolia
- Eocene thrust loading, sedimentation, and convergence in the Sarıcakaya Basin contradict previous interpretations of Eocene slab breakoff

Supporting Information:
- Supporting Information S1
- Data Set S1
- Data Set S2
- Data Set S3
- Data Set S4
- Figure S1
- Figure S2
- Figure S3
- Figure S4

Correspondence to:
M. A. Mueller,
mueller4@uw.edu

Citation:
Mueller, M. A., Licht, A., Campbell, C., Ocakoğlu, F., Taylor, M. H., Burch, L., et al. (2019). Collision chronology along the İzmir-Ankara-Erzincan suture zone: Insights from the Sarıcakaya Basin, western Anatolia. *Tectonics*, *38*, 3652–3674. https://doi.org/10.1029/2019TC005683

Received 23 MAY 2019
Accepted 5 SEP 2019
Accepted article online 10 SEP 2019
Published online 16 OCT 2019

1. Introduction

Anatolia is a complex mosaic of Gondwanan and Laurasian microcontinents that collided from the Late Cretaceous through the Paleogene (Şengör & Yilmaz, 1981). Today, the >1,700-km-long İzmir-Ankara-Erzincan suture zone (İAESZ) demarcates the Pontides in the north from the Anatolide-Tauride Block (ATB) to the south (Figure 1). It is debated whether Pontide-ATB collision was synchronous or diachronous along strike (Kaymakci et al., 2003, 2009; van Hinsbergen et al., 2016). These different models resulted in competitive paleogeographic scenarios requiring unique geodynamic (e.g., Pourteau et al., 2016) and biogeographic (Jones et al., 2018; Métais et al., 2017, 2018; Sen, 2013) reconstructions of the Mediterranean domain and the broader Alpine-Zagros-Himalayan-Tibetan orogen. Synchronous collision models suggest contemporaneous collision in central and western Anatolia whereas diachronous collision models suggest westward younging of collision and suturing across Anatolia (cf. section 2). In western Anatolia, the timing of Pontide-ATB collision is poorly resolved, sometime in the Late Cretaceous, Paleocene, or Early Eocene (e.g., Pourteau et al., 2016). Eocene slab breakoff is inferred from geochemical data (e.g., Altunkaynak, 2007; Dilek & Altunkaynak, 2009; Ersoy, Akal, et al., 2017; Ersoy, Palmer, et al., 2017; Harris et al., 1994; Kasapoğlu et al., 2016; Yildiz et al., 2015) but is either not supported or unresolved in mantle tomography (e.g., Portner et al., 2018; van Hinsbergen et al., 2010) or topographic expression (e.g., Okay et al., 2001; P. Ustaömer et al., 2009). Models consistent with collision or slab breakoff can be tested by examining the stratigraphic record against the expected crustal response. Slab breakoff predicts surface uplift, erosion, and local extension (e.g., Davies & von Blanckenburg, 1995; von Blanckenburg & Davies, 1995), whereas continued underthrusting predicts shortening, basin development, and syntectonic sedimentation.

This study presents the first tectonostratigraphic analysis of the Sarıcakaya Basin in western Anatolia. We refine depositional ages through volcanic zircon U-Pb geochronology, interpret depositional environments from measured sections, and evaluate provenance through detrital zircon U-Pb geochronology and sandstone petrography. We use the Sarıcakaya Basin to appraise models of intercontinental collision and slab breakoff in northwest Turkey and to discuss the implications of our results for geodynamic models of the İAESZ.

2. Geological Context

2.1. Western Anatolian Tectonic Provinces

Northwestern Anatolia encompasses four major tectonic domains, including, from south to north, the Tavşanlı Zone, İAESZ, Sakarya Zone, and Istanbul Zone (Figures 1 and 2).

The ATB zones display distinct and varied metamorphic gradients (van Hinsbergen et al., 2016). The northernmost zone is the Tavşanlı Zone, a mélange of HP/LT blueschist- and eclogite-facies rocks (Okay, 2002). Today, the Tavşanlı Zone comprises, from highest to lowest structural levels, Eocene and Neogene siliciclastic and volcanic rocks of the peripheral Eskişehir foreland basin, obducted Cretaceous ophiolites of the İAESZ, metamorphosed Paleozoic basement, and Late Cretaceous and Eocene-early Oligocene granitoids intruded into the ophiolites and basement (Harris et al., 1994; Okay et al., 1998; Okay & Whitney, 2010; Şengüler & Izladi, 2013; Sherlock et al., 1999). The HT/LP Kırşehir Block in central Anatolia (also known as the Kırşehir Massif or Central Anatolian Crystalline Complex) is arguably either a distinct terrane (e.g., Görür et al., 1984) or the lateral continuation of the Tavşanlı Zone (van Hinsbergen et al., 2016; Plunder et al., 2018; Yaliniz et al., 2000).

North of the Tavşanlı Zone is a highly deformed accretionary prism of metamorphosed oceanic crust and former continental margin units termed the İAESZ. The İAESZ marks the former location of Tethyan oceans that opened and closed in the Mesozoic-Paleogene (Şengör, 1979, and references therein) and consists mainly of ophiolitic mélange, serpentinite, blueschist, and amphibolite rocks (Okay et al., 2002; Okay & Whitney, 2010; Plunder et al., 2013; Sarıfakıoğlu et al., 2017).

The Sakarya Zone of the Pontides is directly north of the İAESZ. The two basement units in the Sakarya Zone are (1) Central Sakarya Basement, composed of Precambrian to Paleozoic crystalline basement, metamorphosed continental units called the Söğüt Metamorphics, and Carboniferous Söğüt granodiorites (also

Figure 1. Generalized and simplified tectonic map of Anatolia (modified from Licht et al., 2017; Pourteau et al., 2013; van Hinsbergen et al., 2016, and references therein). İAES = İzmir-Ankara-Erzincan suture; IPS = Intra-Pontide suture; ITS = Intra-Tauride suture.

termed Söğüt magmatics, Central Sakarya granite, and Sarıcakaya granitoid) (Kibici et al., 2010; Okay, 2000; P. Ustaömer et al., 2012) and (2) the Permian-Triassic subduction-accretion Karakaya Complex composed of metamorphic rocks, ophiolitic mélange, deformed flysch, and limestone (Okay, 2000; Okay & Göncüoglu, 2004; T. Ustaömer et al., 2016). Basement rock units are exposed in south directed thrust sheets and overlain by a thick sequence of unmetamorphosed Jurassic-Miocene sedimentary and volcanic rocks, which are well exposed in the Sarıcakaya and Central Sakarya Basins (Kasapoğlu et al., 2016; Ocakoğlu et al., 2018; Yildiz et al., 2015). North of the İAESZ and Karakaya Complex is the Sarıcakaya Basin (SB), a triangular sedimentary basin (~90 × 0 × 10 km) delimited to the north by the Söğüt Thrust (also termed Nallıhan Thrust), a south directed, basement-involved thrust fault. The thrust fault juxtaposes SB sedimentary units in the footwall under Central Sakarya Basement and Mesozoic-Cenozoic sedimentary units belonging to the forearc-to-foreland Central Sakarya Basin (CSB; also termed the Mudurnu-Göynük Basin) in the hanging wall (Açıkalın et al., 2015, 2016; Altiner et al., 1991; Ocakoğlu et al., 2018; Okay et al., 2001).

The controversial Intra-Pontide Suture Zone, now occupied by the North Anatolian Fault, demarcates the northern extent of the Sakarya Zone from the Istanbul Zone (Akbayram et al., 2016; Robertson & Ustaömer, 2004).

2.2. Evolution of the İzmir-Ankara-Erzincan Suture Zone

Collision in central Anatolia involved three terranes: the Pontides, the Kırşehir Block (KB) and ATB (Figure 1). Based on the wealth of data from central Anatolia, three different collision scenarios are envisaged. (1) In the diachronous promontory collision model, the KB was a promontory of the ATB. Initial collision of the apex of the KB in the latest Cretaceous preceded collision in western and eastern Anatolia (Figure 3a; Floyd et al., 2000; Kaymakci et al., 2003; Meijers et al., 2010; Yaliniz et al., 2000). Ophiolitic belts at the southern KB were from foreland-propagating thrust nappes from the İAESZ not an Intra-Tauride Suture Zone. (2) In a second diachronous model, the soft-hard collision model, the KB was an isolated terrane bounded to the north and south by subduction zones of debated polarity (Görür et al., 1984, 1998; Menant et al., 2016; Robertson et al., 2009). Incipient Pontides-KB "soft" collision in the Maastrichtian-Paleocene was followed by the ATB colliding with southern KB at the Intra-Tauride Suture Zone in a

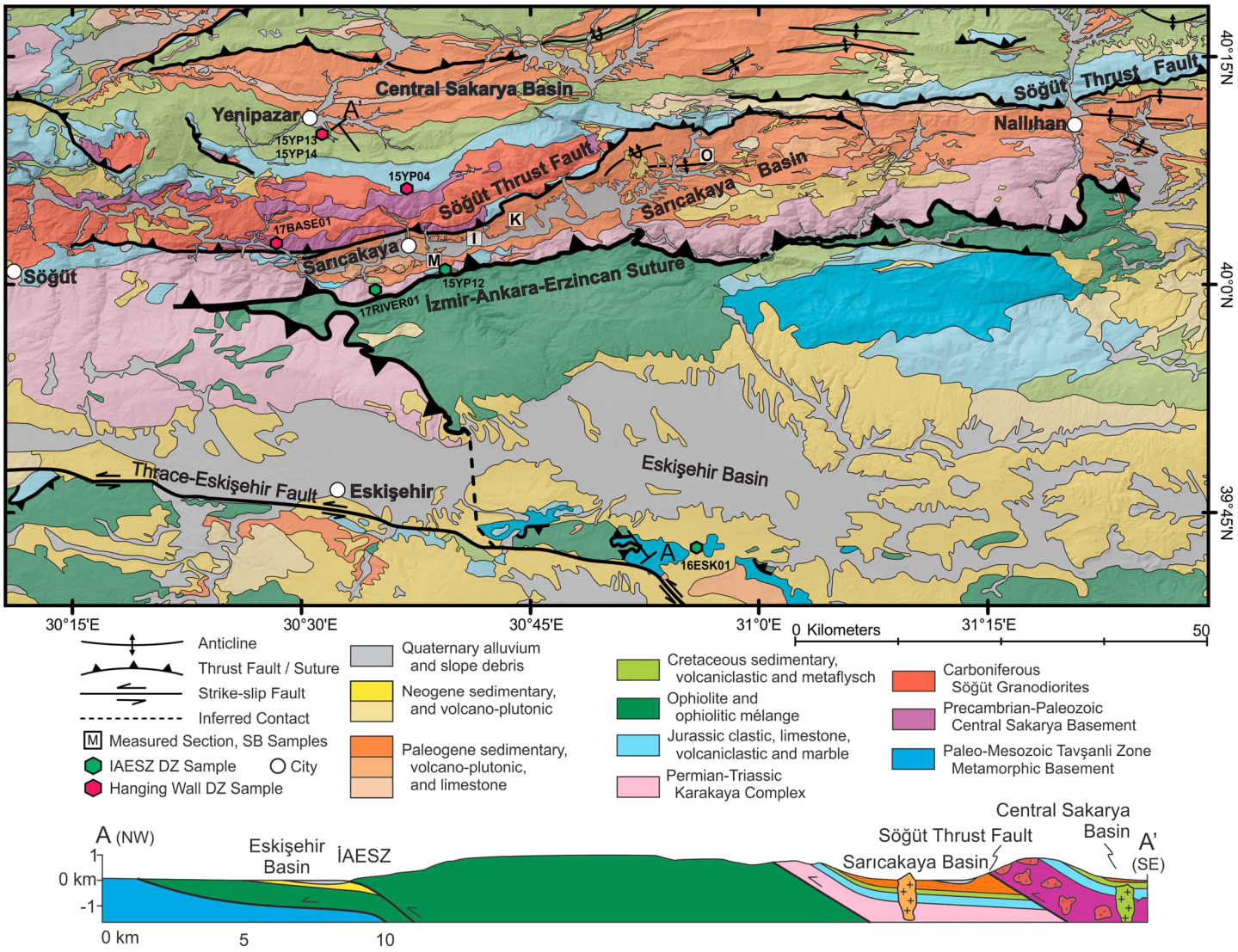

Figure 2. Regional geologic map and schematic cross section of the southern Central Sakarya Basin, Sarıcakaya Basin, İzmir-Ankara-Erzincan suture zone, and Eskişehir Basin (modified from Aksay et al., 2002; Duru & Aksay, 2002; Gedik & Aksay, 2002; Kasapoğlu et al., 2016; Şengüler & Izladi, 2013; Timur & Aksay, 2002; Turhan, 2002 & P. Ustaömer et al., 2012). İAESZ and Söğüt Thrust detrital zircon sample locations are labeled (including those from Campbell, 2017); measured sections locations include SB detrital zircon and sandstone petrography samples (M = Mayıslar sections, I = Iğdir sections, K = Kapıkaya sections, and O = Ozanköy sections). The Paleogene volcano-plutonic unit includes the Nallıhan volcanic rocks and Tavşanlı Zone plutons. See Figure 1 for location.

final, "hard" Eocene collision (Figure 3b; Kaymakci et al., 2009; Licht et al., 2017; Pourteau et al., 2010). The presence of the Intra-Tauride Suture Zone is highly debated (Advokaat et al., 2014; Lefebvre et al., 2013; Menant et al., 2016). In both diachronous models, Pontide-KB collision predated Pontide-ATB collision. (3) The synchronous collision model suggests that the KB was the lateral continuation of the Tavşanlı Zone (Figure 3c). Contemporaneous Paleocene collision of Tavşanlı-KB with the Pontides was followed by a Miocene collision of the eastern ATB with the Pontides (Gürer et al., 2016; Gürer & van Hinsbergen, 2018; van Hinsbergen et al., 2016). Key to this model is the interpretation that contrasting metamorphic grades between the KB and Tavşanlı Zone resulted from NE verging oblique subduction of the KB into an east dipping subduction zone (Lefebvre et al., 2013; Plunder et al., 2018). The synchronous model does not advocate for or against an Intra-Tauride suture but allows for an oceanic basin separating the Tavşanlı-KB from the rest of the ATB.

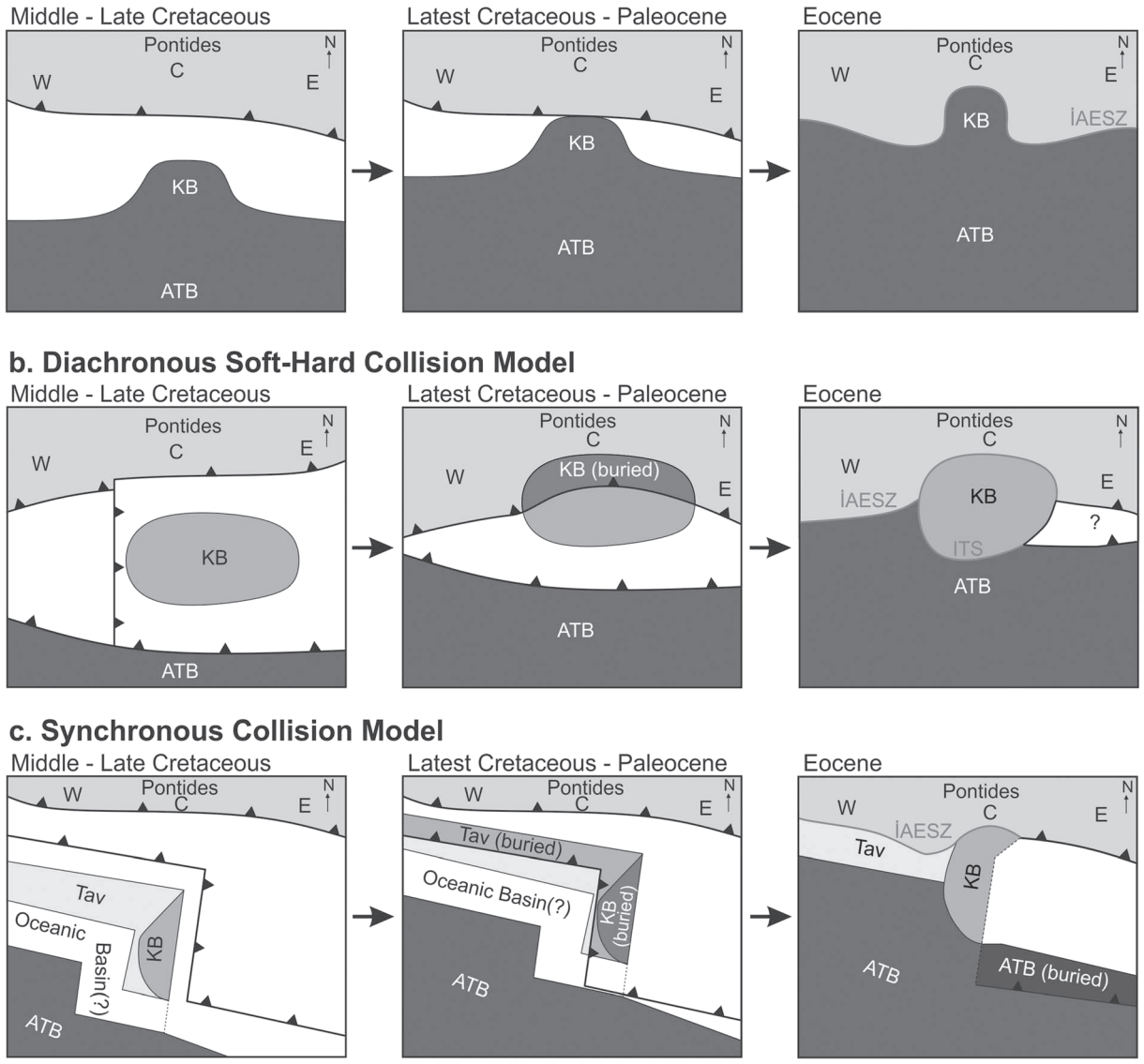

Figure 3. Simplified schematics of various İAESZ evolution models; see text for discussion. (a) Diachronous promontory collision model with the Kırşehir Block as a promontory of the Anatolide-Tauride Block. (b) Diachronous soft-hard collision model with the Kırşehir Block as a distinct terrane bound to the north and south by oceanic basins and subduction zones. (c) Synchronous collision model: the Kırşehir Block and Tavşanlı Zone are connected to the entire ATB and subjected to differing metamorphic conditions during subduction and ophiolite obduction. ATB = Anatolide-Tauride Block; İAESZ = İzmir-Ankara-Erzincan suture zone; ITS = Intra-Tauride suture; KB = Kırşehir Block; Tav = Tavşanlı Zone (part of ATB in a and b).

Several models have been proposed for the evolution of subduction and collision in western Anatolia (Pourteau et al., 2016, and references therein). Regardless of which model is correct, most invoke two Late Cretaceous subduction zones. In the north, the Sakarya Zone was an Andean-type margin (Ocakoğlu et al., 2018; Pourteau et al., 2016), with a volcanic arc occupying E-W trending Campanian extensional structures (Ocakoğlu et al., 2018). In the south, an intraoceanic subduction zone was also active and eventually obducted onto the Tavşanlı Zone, which was itself subducted to blueschist and eclogite facies between 95 and 85 Ma (Okay et al., 1998; Plunder et al., 2013; Pourteau et al., 2010).

The absence of the KB in western Anatolia provides the perfect location to appraise competing Pontide-ATB collisional scenarios. All models agree upon a latest Cretaceous-earliest Paleocene Pontide-KB collision. Therefore, in western Anatolia, a latest Cretaceous-early Paleocene collision would support the synchronous collision model, whereas finding a post-Paleocene collision would support a diachronous suturing model.

2.3. Syncollisional Evolution

The timing of Tavşanlı-Sakarya collision remains imprecise in the literature, with most citing a Late Cretaceous-Eocene collision due to the CSB transition from flysch to molasse (e.g., Göncüoğlu et al., 2000; Okay et al., 1998, 2001; Pourteau et al., 2016). Açıkalın et al. (2016) proposed an early collision at 71 Ma due to the sudden influx of mafic material into the CSB. Yet changes in subduction dynamics or Tavşanlı Zone slab breakoff between 85 and 75 Ma (Okay & Whitney, 2010) could explain precollisional accretionary prism uplift. On the other hand, collision was dated at ~61 Ma based on coeval uplift and an angular unconformity at the southern CSB and prograding deltaic sequences deeper into the basin (Ocakoğlu et al., 2018).

Collision is loosely constrained by structural relationships. Along the suture zone, Paleogene units are the oldest to unconformably overlie both Karakaya Complex and accretionary mélange, indicating that thrust faults juxtaposed the Karakaya Complex and mélange (Figure 2) sometime between deposition of the Upper Cretaceous and lower Paleogene strata (Göncüoğlu et al., 2000) and likely date the age of collision. The east-west trending folds and thin-skinned thrust faults in the CSB and SB comprise the syncollisional Eocene to Mio-Pliocene fold-and-thrust belt (e.g., Okay et al., 2001; Şahin et al., 2019). The most significant thrust is a basement-involved structure, the Söğüt Thrust, which has an along-strike length of ~150-km parallel to the suture zone. At its western end, the Söğüt Thrust juxtaposes Central Sakarya Basement over the Karakaya Complex and Mesozoic-Paleogene sedimentary units. Whereas in the east, Cenozoic sedimentary and volcanic units are in the hanging wall and footwall. Based on a simple linear scaling relationship between fault trace length and amount of displacement, it is reasonable to estimate 15 km of displacement along the ~150-km-long Söğüt Thrust (Cowie & Scholz, 1992; Marrett & Allmendinger, 1991; Walsh & Watterson, 1988). The Söğüt Thrust likely reactivated the paleosuture zone between the accreted Karakaya Complex and the Pontide crystalline basement (Central Sakarya Basement) as there is no Karakaya Complex exposed along the thrust or further north and no Central Sakarya Basement exposed south of the thrust. It would be unlikely for convergent-margin deformation in the accretionary prism to be accommodated along a lithospheric-scale structure like the Söğüt Thrust (e.g., Noda, 2016). Şahin et al. (2019) argue that this fault was syncollisional and active by at least the Eocene but refined dating of the Söğüt Thrust would fine-tune the collision age.

In most places in the SB, the thick Paleogene sedimentary sequence unconformably overlies the Karakaya Complex (Figure 2; Gedik & Aksay, 2002). The basal Paleogene unit is dated from Early Paleocene to Middle Eocene and given various names: the Mihalgazi Formation, including the Çamaklı Member (Yildiz et al., 2015), Kabalar Formation, and Kızılçay Member/Group (Gedik & Aksay, 2002; Kasapoğlu et al., 2016). Uğuz (2013) briefly describes and interprets this unit as debris flow, alluvial fan, flood plain, and lacustrine limestone facies. Based on the rapid Paleocene-Eocene lateral facies changes and coeval magmatism, Göncüoğlu et al. (2000) interpreted the SB as a transtensional basin. Conversely, mapping and structural analysis by Şahin et al. (2019) determined that Paleogene-Miocene units were deposited in a contractional regime.

Volcanism migrated southward from the Late Cretaceous to Eocene (Ocakoğlu et al., 2018). Eocene Nallıhan volcanic rocks are presently between 6- and 10-km north of the İAESZ, implying slab rollback or steepening between the Late Cretaceous and Eocene, perhaps due to syncollisional slowing of the convergence velocity. Here we remain consistent with the published body of literature by using the term "postcollisional" for Eocene magmatism but include it within the "syncollisional" evolution because underthrusting and deformation was active from at least the Cenomanian through Miocene (e.g., Şahin et al., 2019).

The tectonic setting and geodynamic implications of postcollisional magmatism is debated. There are three belts of postcollisional magmatism in western Anatolia: (1) 54- to 48-Ma granodiorite plutons and associated HP/LT metamorphism in the Tavşanlı Zone (Figure 2) (Altunkaynak, 2007; Dilek & Altunkaynak, 2009; Harris et al., 1994; Okay & Satir, 2006; Özdamar et al., 2018), (2) 53- to 47-Ma basaltic to rhyolitic Nallıhan volcanic rocks in the SB and eastern CSB (Figure 2; Harris et al., 1994; Kasapoğlu et al., 2016; Yildiz et al., 2015), and (3) the Kizderbent belt of 53- to 38-Ma volcano-plutonic rocks ~80-km north of the İAESZ (Altunkaynak, 2007; Ersoy, Akal, et al., 2017; Ersoy, Palmer, et al., 2017). Because the Kizderbent volcanic rocks exhibit different geochemical properties (Ersoy, Palmer, et al., 2017) and could belong to a different subduction system (Okay & Satir, 2006), we only consider the Nallıhan and Tavşanlı igneous rocks. Whole rock major and trace elements and Sr–Nd–Pb isotopic compositions of the Nallıhan rocks indicate

some fractional crystallization and crustal contamination, and mixture modeling supports increased asthenospheric (Ersoy, Palmer, et al., 2017) or metasomatized mantle lithospheric sources (Altunkaynak, 2007). The geochemistry, in addition to the linear geometry of the volcano-plutonic belt, the late Paleocene-early Eocene transition from marine to terrestrial deposition (e.g., Okay et al., 2001), and a possible relict slab interpreted from seismic tomography (e.g., Portner et al., 2018; van Hinsbergen et al., 2010) have led many authors to conclude that slab breakoff or delamination processes generated the volcanism (Altunkaynak, 2007; Altunkaynak et al., 2012; Ersoy, Akal, et al., 2017; Kasapoğlu et al., 2016; Yildiz et al., 2015). However, P. Ustaömer et al. (2009) outlined the inconsistencies in the slab breakoff hypothesis, most notably that magmatism from slab breakoff or delamination is emplaced into thickened and elevated crust, yet there was Early-Middle Eocene marine deposition in the three foreland basins. Furthermore, new papers argue that slab breakoff is amagmatic (Garzanti et al., 2018; Niu, 2017). Alternative hypotheses are that the Tavşanlı plutons and Nallıhan volcanic rocks were derived from the mantle wedge or anatexis of the lower continental crust (Harris et al., 1994; Okay et al., 1998), or that magmatism could be explained by migration of the volcanic front toward the suture zone where the crust is thinner (Chapman et al., 2017).

All these different approaches yield contrasting results regarding the timing of Sakarya-Tavşanlı collision and syncollisional deformation and geodynamics. In this part of western Anatolia, the interpretation of slab breakoff has not been tested outside of geochemical analyses. Provenance, deformation, and magmatism have yet to be integrated into a broader model describing collisional evolution. Our work in the Sarıcakaya Basin presents a new holistic model of suturing in this region of western Anatolia.

3. Methods

3.1. Sedimentology

To determine the Paleogene evolution of the Sarıcakaya Basin, we measured 13 stratigraphic sections at decimeter-to-meter resolution at four localities—Mayıslar, İğdir, Kapıkaya, and Ozanköy—in a ~130-km-wide area between Sarıcakaya and Ozanköy (Figure 2), starting at the oldest exposure at the base of the Paleogene series. We subdivide the basin fill into six units and designate informal member names. From the measured sections, we construct a composite stratigraphic section. We describe the sedimentary facies, group them into five main lithofacies, and interpret depositional environments. In our study area, the SB is less than 10-km wide and the Söğüt Thrust has around 15 km of displacement, assuming simple displacement-length scaling relationships (Cowie & Scholz, 1992). Therefore, our stratigraphic sections totaling 1.5 km likely do not reflect significant change in north-south position; in other words, we interpret stratigraphic changes as temporal not spatial evolution because they do not represent any consequential upsection migration toward the thrust front.

3.2. Zircon U-Pb Geochronology

Zircon U-Pb geochronology is used to determine the age of SB sedimentary strata, provenance of the basin sedimentary units, and signatures of potential sediment sources. We collected 12 samples along our stratigraphic sections. Additionally, we analyzed two samples from the İAESZ and one from the Söğüt Thrust hanging wall to characterize the age distributions in these two potential source areas.

The zircon separation, mounting, LA-ICP-MS analysis, and data reduction follow the University of Washington protocol (Licht et al., 2018). Zircons were separated by standard heavy mineral separation methods. A minimum of 140 grains per sample were randomly selected, mounted with standards (Black et al., 2004; Eddy et al., 2016; Sláma et al., 2008), and analyzed using a laser ablation-inductively coupled plasma-mass spectrometer (LA-ICP-MS) at the University of Washington. The data were reduced with *Iolite* using their Geochron Data Reduction Scheme to calculate U-Pb ages uncorrected for common lead (Paton et al., 2011). Individual zircons with >20% discordance, >5% reverse discordance, or abnormal patterns in raw signal intensity were excluded from analyses and interpretations (after Gehrels, 2012, 2014). Crystallization ages of the volcaniclastic zircon samples were determined using *TuffZirc* (Ludwig, 2012). Kernel density estimates were calculated using the plug-in adaptive bandwidth selection method (Botev et al., 2010). Supporting information includes data and detailed analytical protocols.

3.3. Sandstone Petrography

In addition to U-Pb geochronology, we evaluated the provenance of the SB strata from modal sandstone compositions determined through petrographic analysis. Thin sections from 25 fine- to coarse-grained sandstone samples were prepared by National Petrographic Service, Inc. and at the University of Washington. Poorly indurated samples were sieved, and the 63- to 250-μm fractions were mounted in epoxy cups then made into thin sections. At least 340 points per slide were counted using the Gazzi-Dickinson point-counting method (Dickinson, 1985). Ternary diagrams were plotted using *Triplot* (Graham & Midgley, 2000) and interpreted using typical provenance source fields (Dickinson, 1985; Dickinson et al., 1983; Dickinson & Suczek, 1979). Quartz grains include monocrystalline quartz (Qm) and polycrystalline quartz (Qp); feldspar grains (F) include plagioclase and orthoclase; lithic fragments include metamorphic (Lm), sedimentary (Ls; chert, mudstone, siltstone, and sandstone), and volcanic (Lv). Data Set S1 includes the modal data.

4. Results

4.1. Sedimentology of the Eocene Deposits in the Sarıcakaya Basin

We combined individual measured sections into a composite stratigraphic section (Figure 4). There are many small reverse faults throughout the basin, so all measured thicknesses are minimum thicknesses measured from continuous sections. In our study area, contacts between the Karakaya Complex, Jurassic limestone, Cretaceous marine deposits, and Paleogene deposits were reactivated as thrust fault contacts. Growth strata and paleocurrent indicators were not observed, primarily due to faulting, limited exposure, and advanced weathering; weathering also made sedimentary structures difficult to observe. The clastic units are given informal member names and are described from oldest to youngest in the following section: Basal Conglomerate, Lower Lacustrine, Andesitic, Red, Lower Purple, Brown Conglomerate, and Upper Lacustrine Members. We observed depositional contacts between all units (Figures S1–S4); thrust faults in Figure 4 represent small faults observed in some measured section locations. The main lithofacies are synthesized in Table 1.

The Basal Conglomerate Member unconformably overlies Karakaya Complex, Jurassic limestone, or thin remnants of Late Cretaceous marine clastics (Gedik & Aksay, 2002; Timur & Aksay, 2002). The Basal Conglomerate Member is mainly 1- to 3-m-thick massive sets of matrix- and clast-supported conglomerates with very angular serpentinite, chert and greenschist clasts (LF1 in Table 1; Figure 5a). Weakly to strongly calcareous brown mudstones, siltstones, and sandstones are interbedded with the conglomerates.

The base of the Lower Lacustrine Member is made of cross-bedded conglomerate beds interbedded with strongly developed paleosols with root traces and carbonate nodules (LF2), sometimes forming 10- to 50-cm-thick caliches (LF3). The strata then grade into green and gray mudstones and siltstones (LF3), interbedded with 50- to 100-cm-thick white, tabular, and continuous limestone beds (LF4), thick coarse sandstones and isolated conglomerate lenses containing serpentinite, andesitic, and sparse greenschist clasts (LF5).

The Lower Lacustrine Member is capped by the Andesitic Member, which is andesite-bearing volcanic conglomerate beds and massive andesite (Figure 5b). This member is overlain by the Red Member (Figures 5c and 5d), comprising thick red-brown mudstones with gray-green and brown mottling, carbonate nodules, sparse root traces, and isolated greenschist and carbonate clasts (LF2). Typically, the mudstones are capped by either a 50- to 200-cm-thick caliche with isolated clastic matrix (LF3) or 50- to 800-cm-thick tabular and lenticular (5- to 10-m wide) conglomerate beds with clasts of serpentinite, andesite, carbonate, and chert (LF5) (Figure 5d).

The Lower Purple Member is characterized by heavily mottled, carbonaceous purple mudstone (Figure 5e) and siltstone with root traces and isolated clasts (LF2). These mudstones and siltstones are interbedded with $\leq$50-cm-thick organic-rich mudstone and lignite and tabular to lenticular conglomerate and gravel with well-rounded greenschist, quartz, chert, gneiss, schist, and carbonate clasts (LF5; Figure 5f).

The contact between the Lower Purple and Brown Conglomerate Member is an angular unconformity (Figure 5g). The Brown Conglomerate Member is characterized by 1- to 12-m-thick packages of pebble to boulder clast-supported, fining-upward, trough cross-bedded conglomerate with well-rounded clasts of greenschist, carbonate, gneiss, schist, and quartz (LF5; Figures 5h and 5i). Conglomerate troughs are

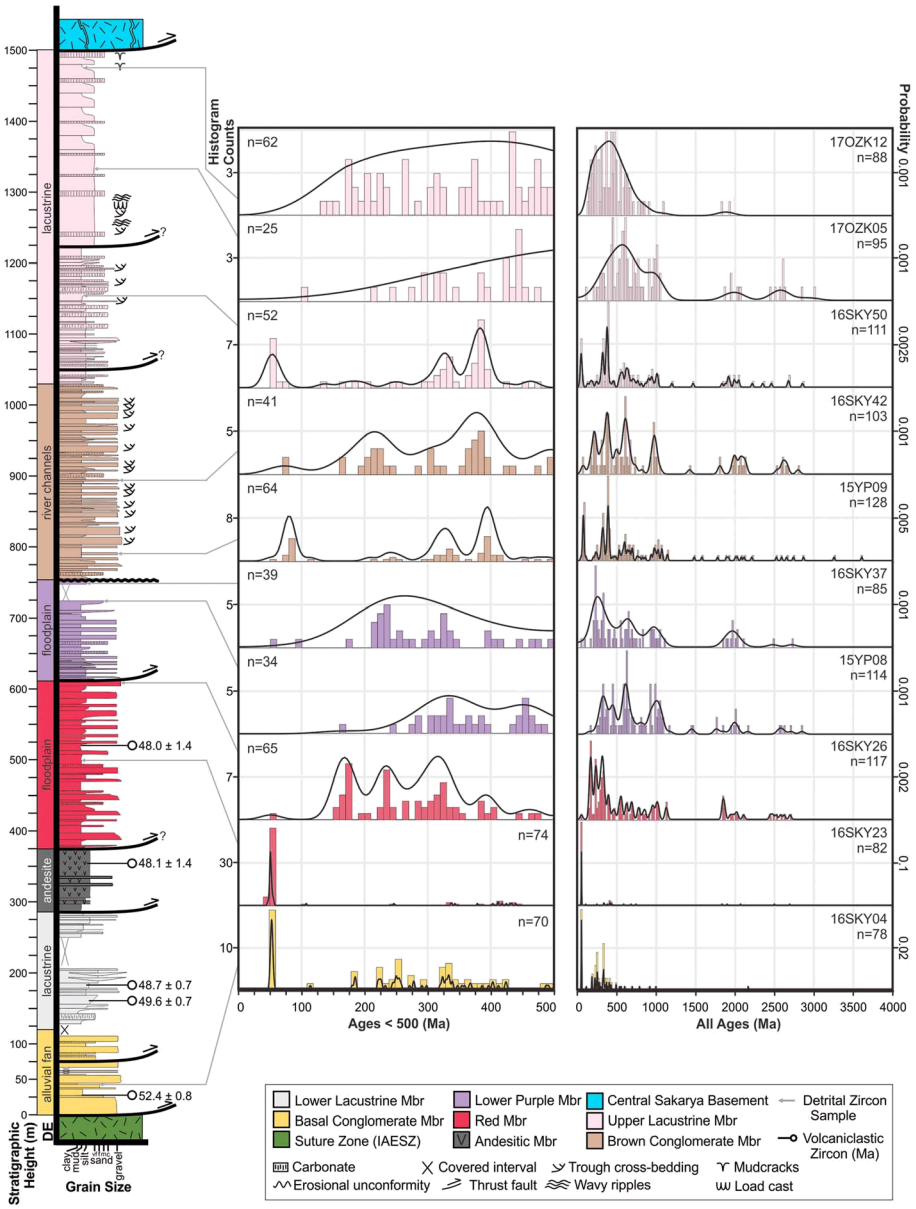

Figure 4. Composite stratigraphic section of the Sarıcakaya Basin with volcaniclastic zircon U-Pb ages. Fill colors correspond with informal members; sedimentary structures symbols and the one fill pattern (carbonate) are defined in the legend. Here observed thrust faults are depicted; see Figures S1–S4 for depositional contacts. The main depositional environment (DE) is given to the left. To the right of the stratigraphic column, histograms, and kernel density estimates (Botev et al., 2010) display detrital zircon age distributions from this study and Campbell (2017). Histograms display all ages in 20-Myr bins in the right column and only ages <500 Ma in 10-Myr bins on the left. Gray arrows connect detrital zircon data to their respective stratigraphic location.

interbedded with mudstones, siltstone, and sandstone with root traces, mottling, pedogenic carbonate nodules, and 50- to 150-cm-thick caliche horizons (LF2; Figure 5j).

The Brown Conglomerate Member vertically transitions into the Upper Lacustrine Member (Figure 5k). Brown-gray mudstone and siltstones with root traces, mottling, pedogenic carbonate nodules (LF2), and 50- to 300-cm caliche (LF3) characterize the basal Upper Lacustrine Member. Additionally, trough cross-bedded conglomerates with quartz, gneiss, greenschist, and carbonate clasts are present (LF5). The top of the Upper Lacustrine Member is red-brown planar laminated very fine, mature (quartz, mica) sand interbedded with mudstone with small, wavy ripples, trough cross lamination, load casts, mudcracks, and trace fossils (Figures 5l and 5m), as well as 5- to 20-cm thick, continuous tabular limestone beds (LF4).

Table 1
Main Lithofacies Identified in the Sarıcakaya Basin

Lithofacies		Description	Members present	Depositional environment interpretation
LF1	Clast-supported conglomerate	Clast-supported, massive conglomerate unit of 1- to 3-m plurimetric sets with very angular, 15- to 100-cm clasts; erosive base; laterally extensive; occasionally matrix supported	Basal Conglomerate	Alluvial fan
LF2	Red-brown mudstone	Red-brown mudstone; structureless, massive, and laterally extensive; root traces, carbonate nodules, isolated clasts, and gray-green to brown mottling; ~1- to 8-m thick; commonly coarsen upward to silt or fine sand and capped by caliche	Lower Lacustrine, Red, Lower Purple, Upper Lacustrine	Pedogenized overbank deposits
LF3	Caliche	10- to 200-cm thick, nodular, massive carbonate horizon, often with isolated clastic matrix	Lower Lacustrine, Red, Lower Purple, Brown Conglomerate, Upper Lacustrine	Paleosol Bk to K horizon
LF4	Tabular limestone	White, tabular, laminated to massive, laterally continuous limestone; 5- to 100-cm thick; afossiliferous	Lower Lacustrine, Upper Lacustrine	Lacustrine limestone
LF5	Trough cross-bedded conglomerate	Pebble- to boulder-sized, clast-supported, well-rounded, trough cross-bedded conglomerate; 1- to 12-m-thick lenticular troughs with erosive base and coarse basal lag that commonly fines upward to coarse sand to cobble conglomerate	Lower Lacustrine, Lower Purple, Brown Conglomerate, Upper Lacustrine	River channels

Note. Lithofacies numbers correspond to those in the text.

4.2. Volcaniclastic Zircon U-Pb Ages

We present the ages of SB volcaniclastic samples in Table 2 and their stratigraphic location in Figure 4. We also include one volcaniclastic sample from Campbell (2017). Volcaniclastic layers are massive, gray-green mudstones predominantly composed of feldspar, which we interpret as weathered pyroclastics (LF3). Zircon grains are angular to rounded, predominantly euhedral, tabular to prismatic, and some grains are broken. The age spectra reveal a single age population (Figure S5; after Vermeesch, 2018) interpreted to reflect a single provenance tied to an eruption event rather than a mixed provenance reflecting recycling from multiple age source areas.

Together, the results constrain deposition of the Basal Conglomerate through Red Members to 52.4 through 48.0 Ma (Figure 4). Results refine the age of these strata as lower Eocene (Ypresian), previously described as upper Paleocene to lower Eocene (Gedik & Aksay, 2002; Yildiz et al., 2015). Deposition was coeval with 53- to 47-Ma Nallıhan volcanism (Kasapoğlu et al., 2016). Maximum depositional ages from sandstones (cf. section 4.3) were also calculated and are compatible with volcaniclastic ages without bringing any additional constraint so are not provided. The age of the Lower Purple through Upper Lacustrine Members is poorly constrained due to the absence of volcanic layers and young zircons. However, laterally correlative deposits in the eastern SB are interbedded with 51.7- to 44.7-Ma lavas and tuffs (Kasapoğlu et al., 2016; Şahin et al., 2019). Therefore, we suspect that our SB sections extend into the middle Eocene.

4.3. Detrital Zircon U-Pb Ages

Detrital zircon grains from eight SB samples ($n = 759$) yielded ages with acceptable concordance and precision for geochronologic interpretation. Within each sample, zircon grains vary from angular to rounded and euhedral to anhedral, and some contain inclusions. The results, plus two detrital samples ($n = 242$) from Campbell (2017), are presented in their stratigraphic position in Figure 4. The 16SKY04 has a prominent Ypresian peak and minor Jurassic, Triassic, and Carboniferous age peaks. The 16SKY23 has a prominent Ypresian age peak. The 16SKY26 has prominent Jurassic, Triassic, and Carboniferous age peaks and a minor Devonian age peak. The 15YP08 has broad Permian-Devonian and Silurian-Ordovician age peaks. The 16SKY37 has a broad Phanerozoic age peak centered around the Triassic-Carboniferous. The 15YP09 has Ypresian, Carboniferous, and Devonian age peaks. The 16SKY42 has broad Jurassic and Devonian age peaks. The 17OZK05 displays a broad peak centering around the late Neoproterozoic. The 17OZK12 only has one broad peak centering around the Devonian and no zircons younger than the earliest Cretaceous. All samples except 16SKY04, 16SKY23, and 17OZK12 have late Neoproterozoic (~600 Ma) and late Mesoproterozoic

Figure 5. Field photographs. (a) Basal conglomerate member with poorly sorted, angular to rounded andesitic and weathered greenschist clasts (LF1). (b) Andesitic Member (sample 16SKY18). (c) View of the Red Member looking toward the west (predominantly LF2) and (d) photograph of lenticular coarse sand to cobble conglomerate with clasts of ophiolitic material, andesite, carbonate, and chert in the Red Member (LF5). (e) Mottled, carbonaceous purple mudstone (LF2/3), and (f) well-rounded to subrounded greenschist, chert, and serpentinite clasts in the Lower Purple Member. (g) View looking toward the north of the Red, Lower Purple, and Brown Conglomerate Members in the Kapıkaya Section. (h) Coarse sand-sized clasts of greenschist, carbonate, gneiss, chert, and quartz in the Brown Conglomerate Member, (i) a trough cross-bedded channel body with rounded boulders (LF5) eroded into a pedogenized brown mudstone (LF2), and (j) a stacked caliche horizon (LF3). (k) View looking toward the west of the Upper Lacustrine Member with laterally continuous, tabular lacustrine limestones (LF5), including (l) mudcracks and (m) trace fossils.

(~1,000 Ma) age zircons. All samples except the two oldest (16SKY04 and 16SKY23) have various minor Paleoproterozoic-late Archean age peaks.

Table 2
Volcaniclastic Zircon U-Pb Ages From the Sarıcakaya Basin

Sample name	Source	Age (Ma)	±2σ abs	±2σ abs incl. modeling error	MSWD	Member	N_0	N
15YP11	Campbell (2017)	52.4	0.6	0.8	0.99	Basal Conglomerate Mbr	98	56
16SKY11	this study	49.6	0.1	0.7	1.30	Lower Lacustrine Mbr	108	20
16SKY18	this study	48.7	0.2	0.7	0.51	Lower Lacustrine Mbr	24	24
16SKY17	this study	48.1	1.3	1.4	0.09	Andesitic Mbr	27	14
16SKY24	this study	48.0	1.2	1.4	0.28	Red Mbr	8	8

Note. Mean square weighted deviation (MSWD) reflects the degree to which the calculated age and uncertainty are representative of a single population. We provide the 2 σ error with and without the 1.3% modelling error (see Text S1 for discussion). 15YP11 is from Campbell (2017); N_0 is the total number of grains; N is the number of grains used in weighted mean age calculation.

The apparent temporal trends in SB samples are the appearance of Precambrian age peaks starting at the top of the Red Member (16SKY26; after 48.0 Ma), the appearance of Late Cretaceous age zircons starting at the top of the Lower Purple Member, and the disappearance of <120- and >2,000-Ma zircons at the top of the Upper Lacustrine Member (17OZK12). These trends are not associated with any trend in depositional environments. A multidimensional scaling map, a visual assessment of misfit between age distributions, is provided in the Supporting Information (Figure S6; Vermeesch, 2013).

We present new (n = 223) and include previously published zircon U-Pb data (n = 769) to characterize provenance source regions (Table 3 and Figure 6). Sample 15YP12, a Karakaya Complex schist, has one prominent Carboniferous age peak (Campbell, 2017). Sample KK.10 is a sandstone sample from the Upper Karakaya Complex in our study region and has prominent late Carboniferous-early Permian and Triassic age peaks (T. Ustaömer et al., 2016). New modern river samples drain the accretionary prism mélange: 17RIVER01 contains minor Carboniferous, Permian, Triassic, and Eocene age peaks, and 16ESK01 has a prominent Carboniferous age peak. Together these samples characterize the İAESZ age distribution. Samples north of the basin characterize the zircon signature of sediment derived from the Söğüt Thrust hanging wall. The sample included from (P. Ustaömer et al., 2012; named here SgtMeta), a sillimanite-garnet schist from Central Sakarya Basement, contains only zircons older than 500 Ma, with two prominent Neoproterozoic age peaks. The 17BASE01 is a new gneiss sample from the Söğüt Metamorphics and has one prominent Ordovician peak. Together, SgtMeta and 17BASE01 characterize the Central Sakarya Basement signature. Central Sakarya Basin detrital sandstone samples from Ocakoğlu et al. (2018) and Campbell (2017) are included to characterize the sedimentary strata of the Söğüt Thrust hanging wall that could be reworked and deposited in the SB. Jurassic 15YP04 has one Carboniferous age peak, Upper Cretaceous sample 15YP13 contains one prominent Campanian peak, and Upper Cretaceous 15GO02 and Paleocene-Eocene(?) 15YP14 have a prominent Campanian age peaks and a minor Carboniferous peak.

Next, we grouped all samples by location—north (Söğüt Thrust hanging wall) and south (İAESZ) of the SB—to evaluate the similarity and relative contribution of each source area to the SB strata (Figure 7). Therefore, we plot both all Söğüt Thrust hanging wall samples and only Central Sakarya Basement samples (no Mesozoic-Cenozoic sedimentary samples), and all İAESZ samples and only Karakaya Complex samples. The Central Sakarya Basement has characteristic age peaks >450 Ma. The signal from the Late Cretaceous arc is unique to the Upper Cretaceous and Paleo-Eocene(?) sedimentary samples in the Söğüt Thrust compilation. The Triassic age peak is characteristic of the Karakaya Complex.

4.4. Sandstone Petrography

The modal framework grain composition of 25 SB samples is shown in four ternary diagrams (Figure 8). The majority of samples classify as lithic, quartzo-lithic, and litho-quartzose sandstones with <10% feldspar and varying proportions of quartz and lithic grains (after Garzanti, 2018); three lower lacustrine member samples contain larger proportions of feldspar. Most samples plot within the recycled orogen and magmatic arc province fields. The Red through Upper Lacustrine Members display a trend of increasing proportions of monocrystalline and polycrystalline quartz. On average, accessory minerals, including

Table 3
Detrital Zircon U-Pb Samples From This Study and From Previously Published Sources Categorized by Provenance Source Regions

Sample name	Source	Provenance category	Stratigraphic unit and lithology
15YP12	Campbell (2017)	IAESZ	Upper Karakaya Complex greenschist
KK.10	T. Ustaömer et al. (2016)	IAESZ	Upper Triassic Kendirli Fm (Karakaya Complex) sandstone
17RIVER01	this study	IAESZ	Modern river sand draining the accretionary prism into Sarıcakaya Basin
16ESK01	this study	IAESZ	Modern river sample draining accretionary prism and Karakaya Complex
16SKY04	this study	Sarıcakaya Basin	Basal Conglomerate Mbr sandstone
16SKY23	this study	Sarıcakaya Basin	Red Mbr sandstone
16SKY26	this study	Sarıcakaya Basin	Red Mbr sandstone
15YP08	Campbell (2017)	Sarıcakaya Basin	Lower Purple Mbr sandstone
16SKY37	this study	Sarıcakaya Basin	Lower Purple Mbr sandstone
15YP09	Campbell (2017)	Sarıcakaya Basin	Brown Conglomerate Mbr sandstone
16SKY42	this study	Sarıcakaya Basin	Brown Conglomerate Mbr sandstone
16SKY50	this study	Sarıcakaya Basin	Upper Lacustrine Mbr sandstone
17OZK05	this study	Sarıcakaya Basin	Upper Lacustrine Mbr sandstone
17OZK12	this study	Sarıcakaya Basin	Upper Lacustrine Mbr sandstone
SgtMeta	P. Ustaömer et al. (2012)	Söğüt Thrust Hanging Wall	Central Sakarya Basement sillimanite-garnet schist
17BASE01	this study	Söğüt Thrust Hanging Wall	Gneiss from the Söğüt Metamorphics
15YP04	Campbell (2017)	Söğüt Thrust Hanging Wall	Jurassic Bilecik Fm sandstone
15YP13	Campbell (2017)	Söğüt Thrust Hanging Wall	Upper Cretaceous Yenipazar Fm sandstone
15GO02	Campbell (2017) and Ocakoğlu et al. (2018)	Söğüt Thrust Hanging Wall	Upper Cretaceous Yenipazar Fm conglomerate
15YP14	Campbell (2017)	Söğüt Thrust Hanging Wall	Paleogene Kizilçay Fm sandstone

epidote, white mica, biotite, zircon, serpentine, amphibole, calcite, and opaque minerals, comprise 10%–30% of total framework grains.

5. Interpretation

5.1. Depositional Environments

The Sarıcakaya Basin sedimentary facies reflect three main depositional environments: alluvial fan, fluvial (channels and floodplain), and lacustrine. There is no evidence for marine deposition.

Laterally extensive, clast-supported, massive conglomerate beds with very angular clasts and an erosive base, interbedded with medium-to-coarse sandstone and mudstone, are interpreted as debris flow deposits on alluvial fans (LF1; Table 1; Nichols, 2009; Prothero & Schwab, 1996). Massive, matrix-supported conglomerates are interpreted as proximal fluvial and sheetflood deposits within alluvial fans (LF1; Nichols, 2009). Structureless, red-brown mudstones are massive and laterally extensive; they commonly coarse upward and are capped by caliche. Due to the abundant root traces, carbonate nodules, mottling, we interpret these facies as pedogenized overbank deposits (LF2; Retallack, 1988). Continuous, tabular, unfossiliferous, and laminated limestones can be easily distinguished from massive, nodular caliches (LF3) and are interpreted as lacustrine limestones (LF4; Prothero & Schwab, 1996). Conglomerate and sandstone bodies display the characteristic wing shape and fining upward sequence with erosive, coarse basal lags found in fluvial channel bodies (LF5; Nichols, 2009).

Overall, the depositional environments reflect long-term, repetitive changes along an alluvial fan-floodplain-lake system. The juxtaposition of well-developed soil horizons on top of alluvial fans and fluvial channels suggests frequent alluvial fan lobe and fluvial channel avulsions. Lacustrine limestone formation suggests periods of low sedimentary input.

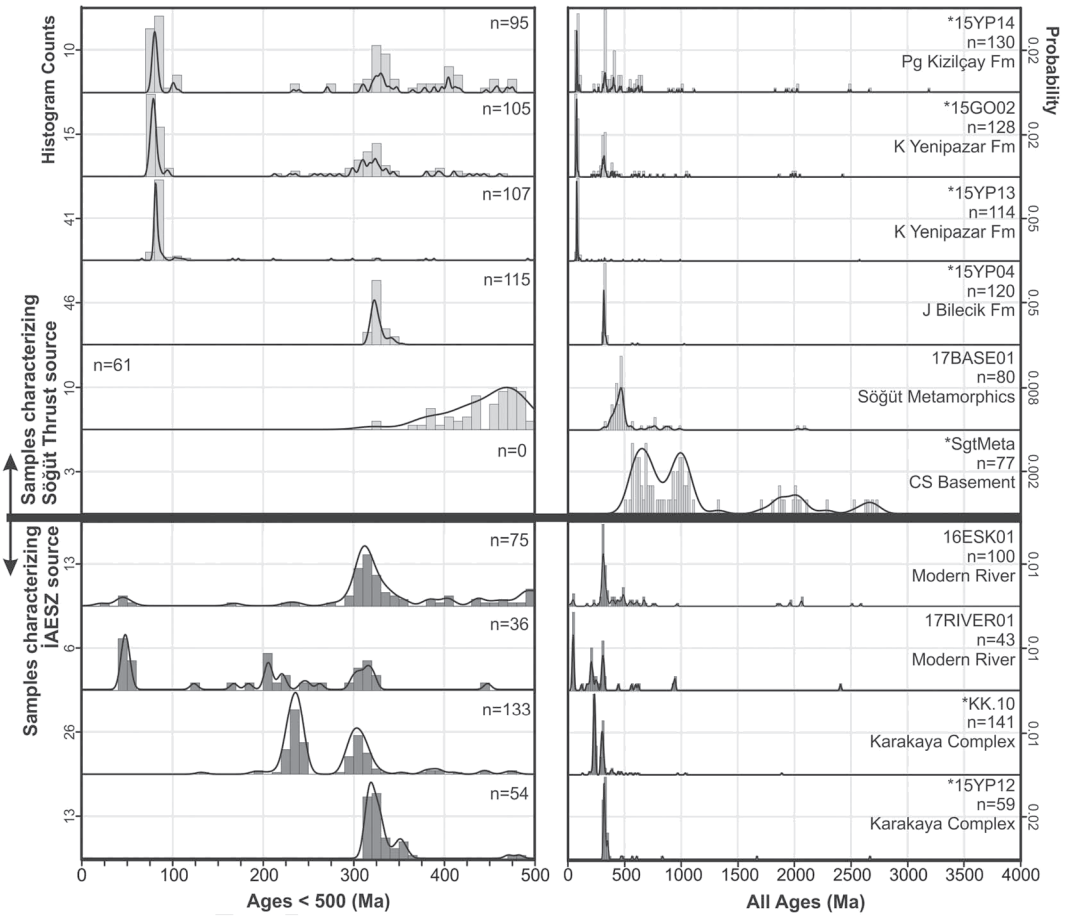

Figure 6. Histograms and kernel density estimate diagrams for detrital zircon age distributions of samples characterizing potential Sarıcakaya Basin sedimentary sources. Samples are grouped by potential source regions and stacked in stratigraphic order: Sedimentary units and Central Sakarya Basement of Söğüt Thrust hanging wall (light gray, top) characterize sediment derived from the north; Karakaya Complex and modern rivers draining the İAESZ characterize the south (dark gray, bottom). All ages are displayed in the right column in 20-Myr bins and only ages <500 Ma in 10-Myr bins on the left. CS = Central Sakarya; J = Jurassic; K = Cretaceous; Pg = Paleogene; * previously published data (Table 3).

5.2. Sedimentary Provenance

The provenance results from detrital zircon, modal sandstone, and field observations establish that the SB sediments contain detritus sourced from the İzmir-Ankara-Erzincan suture zone and Söğüt Thrust fault hanging wall.

5.2.1. Detrital Zircon U-Pb Geochronology

Here we interpret the source of zircons found in SB samples, from oldest to youngest, based on the comparison with potential sediment sources (Figure 7). Early Paleozoic and Precambrian zircons present in SB samples younger than 48.0 Ma are derived from exposed Central Sakarya Basement. Minor Proterozoic peaks present in the SB are not present in the two source compilations, such as the 1,500-Ma peak (0.5%). This could indicate that there were other sedimentary sources, or it could be an artifact of sample size. The Devonian age peak (~400 Ma) is not useful for provenance because it is present in both sources. Similarly, our data set does not determine whether Carboniferous zircons in the SB are from Central Sakarya Basement exposed by the Söğüt Thrust, Karakaya Complex, or reworked Söğüt Thrust sedimentary strata. Triassic zircons are abundant in the SB and İAESZ (especially KK.10) and minorly present in the post-Jurassic Söğüt Thrust samples (2.7%). We suggest that Triassic zircons in the SB reflect sediment input from the Karakaya Complex in the suture zone. Jurassic zircons in the SB do not appear to be derived from either potential source. The Late Cretaceous zircons are present in the post-Jurassic Söğüt Thrust sedimentary samples and in most SB samples younger than 48.0 Ma. These zircons could come directly from the

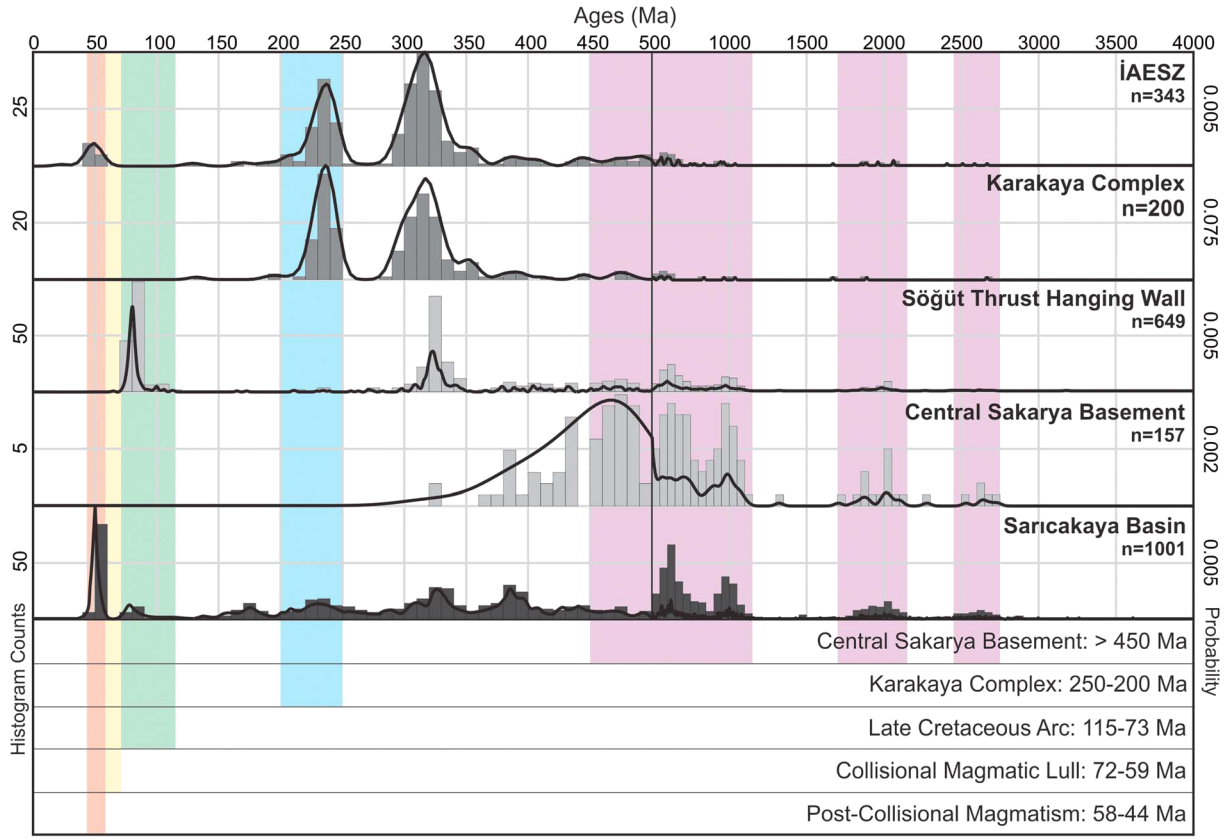

Figure 7. Histograms and kernel density estimate diagrams of sample groups: Sarıcakaya Basin (dark gray), Söğüt Thrust hanging wall and only Central Sakarya Basement samples (light gray), and İAESZ and only Karakaya Complex samples (medium gray). Colored bars highlight both Cretaceous-Paleogene magmatic cyclicity, and age peaks diagnostic of SB provenance. Histograms are in 10-Myr bins for ages <500 Ma, and 50-Myr bins for ages >500 Ma.

Cretaceous volcanic arc in the CSB or Beypazarı plutons or reworked Söğüt Thrust hanging wall. Eocene volcanism is well documented within the SB; therefore, Eocene zircons likely reflect sediment or ash derived directly from the arc. The Eocene age peak in the İAESZ samples could be from Nallıhan volcanic rocks or Tavşanlı plutons.

We summarize and interpret the provenance data as follows. The oldest SB detrital zircon sample (Basal Conglomerate Member) contains Triassic zircons, which are characteristic of Karakaya Complex, and almost no pre-Carboniferous zircons, suggesting a predominant input of material from the İAESZ and locally from the Nallıhan volcanics around 52.4 Ma. The dominance of the Eocene peak in 16SKY23 suggests continued sediment sourcing from the Nallıhan arc through 48.0 Ma. There is a change in provenance around 48.0 Ma. Samples from the Red through Upper Lacustrine Members contain age peaks uniquely associated with the Central Sakarya Basement (>450 Ma). This signal demonstrates that Central Sakarya Basement was exposed along the Söğüt Thrust by 48.0 Ma, and the continued presence of Triassic age zircons demonstrates sustained input from the İAESZ.

5.2.2. Sandstone Petrography and Clast Composition

Modal sandstone compositions affirm the same provenance trends as the detrital zircon data (Figure 8). The Basal Conglomerate through Red Members samples plot in the oceanic affinity region of the recycled orogenic province or volcanic arc province. Lower Purple through Upper Lacustrine Members demonstrate an upsection increase in quartz and plot in the mixed or continental affinity region of the recycled orogenic province, especially the Brown Conglomerate and Upper Lacustrine Members. The İAESZ lithologies are low in quartz and feldspar unlike the exposed Central Sakarya Basement and overlying sedimentary units. Therefore, we interpret the upsection trend as an increase in sediment supply from the Söğüt Thrust

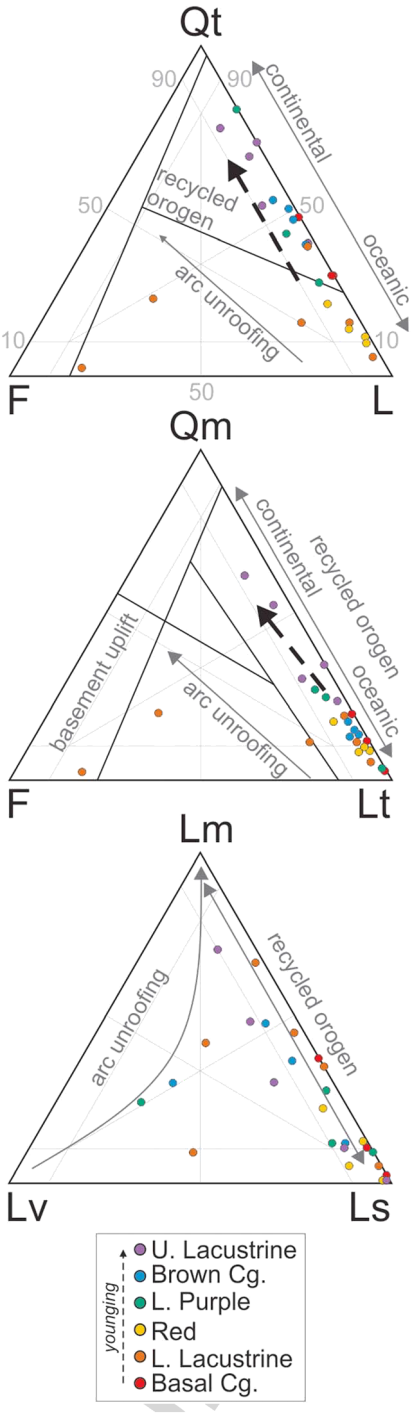

Figure 8. Ternary diagrams of sandstone modal framework-grain composition from the Sarıcakaya Basin showing petrographic ranges of typical source provinces following Dickinson (1985) and Dickinson and Suczek (1979) updated by Garzanti (2018). Points are colored by informal sedimentary members. Black dashed arrows indicate general upsection trends where present. Province fields and trends are labeled with dark gray text and arrows. Light gray lines and numbers label the axes. Ternary diagram poles —Qt = total quartz (Qm = monocrystalline quartz and Qp = polycrystalline quartz), F = total feldspar, L = lithic fragments (Lm = metamorphic, Ls = sedimentary, Lv = volcanic, Lt = total lithic fragments including polycrystalline quartz).

hanging wall. The dominance of sedimentary lithics suggests that material was reworked from the İAESZ, Söğüt Thrust, and/or within the SB.

Field observations suggest similar changes in conglomerate clast compositions upsection, from predominantly greenschist, serpentine, red radiolarian chert, and andesitic clasts in the lower half of the section to mostly quartz, gneiss, and schist in the upper half. Field observations suggest that carbonate clasts are derived from two sources: eroded and reworked caliche and lacustrine limestone and from Jurassic limestone. Reworked carbonate clasts indicate progressive deformation of sedimentary strata in the SB, supporting syntectonic deposition.

5.3. History and Origin of the Sarıcakaya Basin

In this section, we synthesize geochronologic, provenance, and sedimentologic data to describe the origin and evolution of the Sarıcakaya Basin. We conclude that the SB was a broken foreland basin formed by flexural loading from the Söğüt Thrust.

We used volcaniclastic U-Pb ages to determine that the oldest exposed Paleogene deposits are ~52.4 Ma. Therefore, the SB was set up by at least 52 Ma and deposition continued through at least 48 Ma. Deposition was coeval with postcollisional magmatism. Because there were no tuffs to constrain the upper age of our section, the duration of deposition is uncertain. Correlative deposits in the eastern SB are interbedded with 51.7- to 44.7-Ma lavas and tuffs, and our section is entirely terrestrial, so it is possible that our section captures at least the early Lutetian prior to the late Lutetian-Bartonian/Priabonian (?) marine incursion (Ocakoğlu et al., 2012, 2018; Şahin et al., 2019).

All provenance data are consistent with the SB system being fed by the hanging wall of the Söğüt Thrust

and İAESZ. Detrital zircon and sandstone petrography results display a similar trend of increasing relative proportions of Central Sakarya Basement material, starting at the top of the Red Member around 48.0 Ma. The presence of Central Sakarya Basement material demonstrates that the Söğüt Thrust was active and accommodating syncollisional convergence by at least 48 Ma.

The presence of a sedimentary basin requires a mechanism of formation and accommodation space creation. Models for sedimentation in foreland basins correlate periods of fold-and-thrust belt buildup (flexural loading) to depositional environments. It is debated whether coarse-grained deposition in foreland basins reflects periods of tectonic activity in the fold-and-thrust belt or isostatic adjustment and progradation during fold-and-thrust belt quiescence. Either (1) tectonically driven uplift and erosion increases subsidence rate, sediment flux, and grain size (Burbank et al., 1988; Heller & Paola, 1992; Paola et al., 1992) or (2) periods of rapid tectonic loading from fold-and-thrust belt activity flex the crust and increase both accommodation space and subsidence rates to drive fine-grained deposition (deeper facies) in the basin (Flemings & Jordan, 1990; Heller & Paola, 1992; Paola et al., 1992). Neither model is universally applicable (Burbank et al., 1988), but both confirm that the repetitive change between coarse- and fine-grained deposition is characteristic of thrust-loading flexural basins.

The provenance data support an active thrust and repetitive changes from coarse-grained alluvial fan and fluvial channel facies to fined-grained overbank and lake facies (Figure 4) by 48.0 Ma. Therefore, we classify the SB as a Laramide-style broken foreland basin by 48.0 Ma (Dickinson et al., 1988). We argue that the SB was likely formed as a broken foreland basin as early as 52.4 Ma because the same repetitive change in depositional environments are present by 52.4 Ma. The delay in Central Sakarya Basement material in the zircon results and in quartz-rich compositions until around 48.0 Ma can be explained in two ways. First, we measured section along the southern limb of the basin; it would have taken some to overfill the basin such that material from the northern limb reached the southern limb. Second, based on measured sections (Ocakoğlu et al., 2018), field observations and local geologic maps (Duru & Aksay, 2002; Gedik & Aksay, 2002; Timur & Aksay, 2002), there was at least 2 km of Jurassic-Cretaceous sedimentary cover at the southern margin of the CSB. Therefore, there must have been at least 2 km of throw and correlative erosion on the Söğüt Thrust by about 48.0 Ma to shed basement-derived zircons into the SB.

6. Discussion

6.1. Western İzmir-Ankara-Erzincan Suturing and Geodynamics

6.1.1. Sakarya-Tavşanlı Collision

We refine the age of Sakarya-Tavşanlı collision via two pieces of evidence. First, we constrain the minimum age for the onset of syncollisional deformation to 52.4 Ma. Yet, collision was likely much earlier because the Söğüt Thrust must have been active before the onset of deposition in the SB. Second, the timing of collision is further constrained by our geochronologic dataset of magmatic flare-ups and lulls in western Anatolia near the İAESZ: 73- to 115-Ma magmatism, 59- to 72-Ma lull, and 44- to 58-Ma magmatism. This magmatic cyclicity suggests that the Late Cretaceous arc was active until 72 Ma and collision occurred sometime in the Maastrichtian-Middle Paleocene. This 72- to 59-Ma lull is compatible with both ages previously proposed in western Anatolia, 71 and 61 Ma (Açıkalın et al., 2016; Ocakoğlu et al., 2018), and with the age of collision in central Anatolia (e.g., Kaymakci et al., 2009).

6.1.2. Slab Dynamics in Western Anatolia

Without conclusive mantle tomography, slab breakoff must be identified by its surface expression: uplift, local extension, and extensional exhumation. No Paleogene extensional features have been described. There are three periods of uplift and erosion that could be correlated to slab breakoff. (1) The SB and CSB Paleogene deposits are in angular unconformity with underlying units (Ocakoğlu et al., 2018; Şahin et al., 2019). Therefore, there was uplift and erosion sometime between the Late Cretaceous and 52 Ma, during a magmatic lull. If slab breakoff is amagmatic (Garzanti et al., 2018; Niu, 2017), then this period could encompass initial Tavşanlı-Sakarya collision, slab rollback, and/or steepening and slab breakoff. This is the best candidate for slab breakoff, and this scenario does not change the interpretation of the Eocene SB. (2) Our data demonstrate there was uplift and erosion at the southern and northern SB coeval with postcollisional magmatism. Yet, the Söğüt Thrust was accommodating shortening in the Paleogene (Şahin et al., 2019) and the Central Sakarya Basement was exposed by the Ypresian. The SB could not have formed during an extensional regime: the Söğüt Thrust is the boundary between Karakaya Complex and Central Sakarya

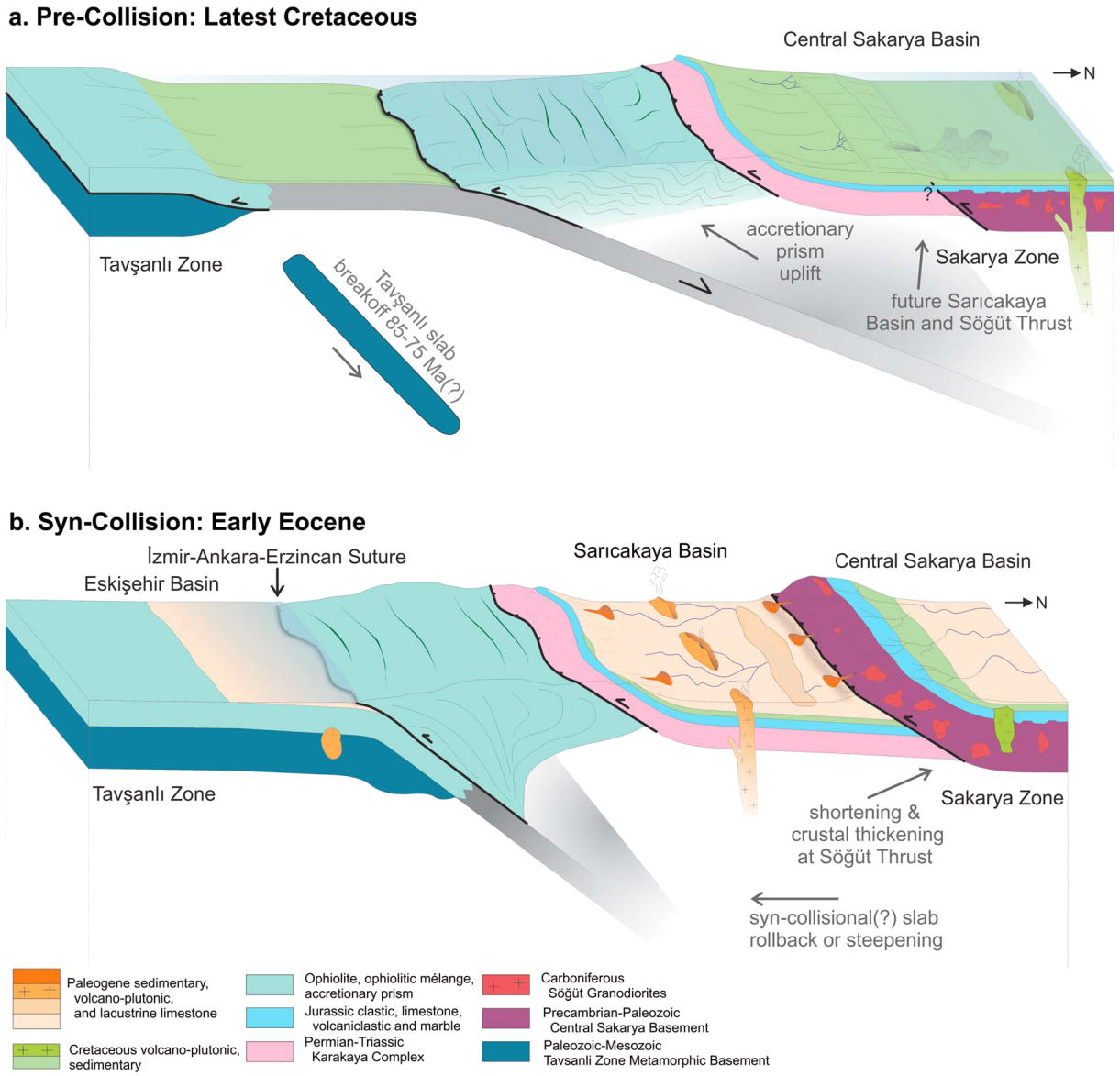

Figure 9. Conceptual model of the Sarıcakaya, Eskişehir, and Central Sakarya Basins and İzmir-Ankara-Erzincan suture zone. See text for detailed discussion and Figure 1 for location. (a) Reconstruction of the İzmir-Ankara subduction zone in the latest Cretaceous prior to collision of the Sakarya Zone with the Tavşanlı Zone at 66 Ma. (b) Reconstruction of the Sarıcakaya Basin in the Early Eocene (~52–47 Ma) based on interpreted depositional environments and provenance.

Basement, so any extension along this structure would not expose Central Sakarya Basement. (3) The angular unconformity at the base of the Brown Conglomerate Member likely reflects a period of uplift and erosion. The unconformity is poorly constrained to younger than 48.0 Ma. There is no clear change in depositional style or provenance before and after the unconformity. There is no evidence to suggest the unconformity represents a long period of major uplift, exhumation, and erosion.

Based on the contractional regime in the Early Eocene, we prefer the interpretation that the Nallıhan and Tavşanlı igneous rocks are consistent with continued underthrusting, southward mantle wedge migration, and magmatism, as opposed to slab breakoff, lithospheric delamination, or arc root foundering (Figure 9). Syncollisional convergence is facilitated by continued slab pull from the Tavşanlı slab and/or a southward jump in subduction to the Afyon-Tavşanlı Zone interface or the northern margin of the African plate (Figure 1; e.g., Pourteau et al., 2016). There was ~250 km of convergence between Africa and Europe from 50 to 35 Ma (van Hinsbergen et al., 2010). If the Söğüt Thrust only accommodated 15 km of convergence,

faults in the accretionary prism and/or the Intra-Pontide suture, in addition to southern active subduction zones, might have accommodated a significant amount of shortening.

The geochemical signature of the Nallıhan and Tavşanlı igneous rocks is interpreted as from an asthenospheric (Ersoy, Palmer, et al., 2017) or metasomatized lithospheric mantle source (Altunkaynak, 2007). Alternatively, the magmatic rocks could be the result of several factors other than slab breakoff. First, the Sakarya Zone, a rifted terrane (P. Ustaömer et al., 2012), could have been thin in the Eocene, as the Tavşanlı Zone crust was only 30-km thick at that time (Okay et al., 1998). Second, if the Söğüt Thrust marks the boundary between Central Sakarya Basement and Karakaya Complex, then the crust beneath the SB was thin and oceanic, explaining why there was little crustal contamination (Altunkaynak, 2007). Lastly, the Eocene volcanic front, located within 5 km of the accretionary mélange, could have been derived from the mantle wedge (Harris et al., 1994; Okay et al., 1998).

6.2. Geodynamic Model

In this section, we synthesize the Sarıcakaya Basin interpretation into a holistic model for the evolution of this part of western Anatolia (Figure 9).

1. Prior to Sakarya-Tavşanlı collision, the CSB was one large forearc-backarc basin complex bisected by the Late Cretaceous volcanic arc (Açıkalın et al., 2016; Ocakoğlu et al., 2018).
2. Initial collision in the Maastrichtian-Middle Paleocene was marked by a magmatic lull (72–59 Ma; Figure 7). Collision was marked in the CSB stratigraphic record as uplift, northward deltaic progradation, shallowing, increased sedimentation rates, and an angular unconformity (Ocakoğlu et al., 2018). Shortening and underthrusting were accommodated by the Söğüt Thrust, the paleosuture between Karakaya Complex and Central Sakarya Basement. There was syncollisional slab rollback.
3. By 52 Ma, the SB formed by flexural loading from Söğüt Thrust and was partitioned from the CSB. Sediment was initially sourced from the volcanic arc and suture zone and likely the sedimentary cover in the Söğüt Thrust hanging wall. Around 48.0 Ma, Central Sakarya Basement was exposed along the thrust and feeding the SB. Postcollisional Nallıhan and Tavşanlı magmatism occurred over a 14-Myr span, from 58 to 44 Ma. The slab was steeply dipping, evidenced by the short distance from the suture zone to volcanic front.

6.3. Central-Western Anatolian Geodynamics

The three collision models for central Anatolia estimate Pontides-Kırşehir Block collision was in the Maastrichtian-early Paleocene based on stratigraphic, metamorphic, magmatic, and structural analyses (Görür et al., 1984, 1998; van Hinsbergen et al., 2016; Kaymakci et al., 2009; Lefebvre et al., 2013; Licht et al., 2017; Meijers et al., 2010; Robertson et al., 2009). Here we affirm a Maastrichtian-Middle Paleocene collision in western Anatolia, supporting the synchronous collision model (e.g., Gürer & van Hinsbergen, 2018).

Furthermore, there is coeval deformation and basin formation along the İAESZ. We demonstrate fold-and-thrust belt development and basin formation by 52 Ma. Large Cretaceous-Eocene peripheral and retro-arc foreland basins and fold-and-thrust belts developed in central Anatolia (Hippolyte et al., 2016; Janbu et al., 2007; Leren et al., 2007) and generally recorded a switch from Late Cretaceous extension to syncollisional contraction in the Paleocene-Early Eocene (Kaymakci et al., 2009; Nairn et al., 2013). There are a few differences, such as, after collision in central Anatolia, deformation fronts of thin-skinned thrust belts and depocenters migrated perpendicularly away from the suture zone (Advokaat et al., 2014; Kaymakci et al., 2009) as opposed to deposition in the SB near the suture zone. Also, thick-skinned deformation in the west preceded Middle-Late Eocene thick-skinned deformation in central Anatolia (e.g., Kaymakci et al., 2009; Nairn et al., 2013). This along-strike change in deformation remains unexplained in collision models but could be a result of changes in lithology, basement thickness, preexisting structures, or effects of oblique subduction on orogen dynamics (Plunder et al., 2018).

In addition, magmatic flare-ups and lulls were synchronous along the İAESZ. From a large, compiled data set (n = 702) of <100-Ma magmatism in central and eastern Anatolia, Schleiffarth et al. (2018) find a high-flux magmatic event from 73 to 100 Ma, magmatic lull from 60 to 72 Ma, and flare-up from 40 to 58 Ma. This is almost exactly the results of our data set (n = 2,245): 73- to 115-Ma magmatism, 59- to 72-Ma lull, and 44- to 58-Ma magmatism.

Contemporaneous collision, deformation, and magmatism across the western and central İAESZ all suggest that the synchronous collision model is the most suitable. Our data and interpretations of the SB are more aligned with a coeval collision of the KB and Tavşanlı Zone with the Pontides, suggesting that the KB is the lateral equivalent of the Tavşanlı Zone and not a promontory or separate terrane.

7. Conclusions

We constrain Pontide-Tavşanlı Zone collision to Maastrichtian-Middle Paleocene. We demonstrate that the Sarıcakaya Basin was a syncollisional, Eocene broken foreland basin that formed by flexural loading from the Söğüt Thrust by 52 Ma. Sediment was sourced from both the İzmir-Ankara-Erzincan suture zone and basement-involved Söğüt Thrust. The SB cautions against the overuse of slab breakoff to explain postcollisional magmatism (Garzanti et al., 2018; Niu, 2017). Our reconstruction of the SB elucidates complete opposite crustal response than what is predicted by slab breakoff. The SB formed in contractional regime, with significant basin subsidence coeval with postcollisional magmatism. We provide a new model of syncollisional evolution in western Anatolia in which convergence, underthrusting, and accommodation space creation dominate during the early Eocene. Compared to the record of collisional evolution in central Anatolia, we demonstrate a synchronous magmatic history and onset of deformation along the İzmir-Ankara-Erzincan suture zone. Contemporaneous collision supports synchronous collision models which imply the Kırşehir Block was the lateral continuation of the Tavşanlı Zone not an independent terrane or promontory.

Acknowledgments
This research was funded by the U.S. National Science Foundation (EAR-1543684). Raw data and additional files supporting our analyses and conclusions are in the Supporting Information and a Mendeley Data repository (https://data.mendeley.com/datasets/vs292g83c4). Thoughtful reviews by N. Lom and M. Darin improved this manuscript. We thank K. W. Huntington, M.D. Turzewski, M. Wood, P. Ballato, Ç. Ocakoğlu, M.Z. McIntire, D.S. Cowan, J.G. Crider, S. Kuehner, P. Schoettle-Greene, C.D. Rowe, and D. McDougall for their prolific discussions and assistance in the field and in the lab.

References

Açıkalın, S., Ocakoğlu, F., Yılmaz, İ. Ö., Vonhof, H., Hakyemez, A., & Smit, J. (2016). Stable isotopes and geochemistry of a Campanian-Maastrichtian pelagic succession, Mudurnu–Göynük Basin, NW Turkey: Implications for palaeoceanography, palaeoclimate and sea-level fluctuations. *Palaeogeography, Palaeoclimatology, Palaeoecology*, *441*, 453–466. https://doi.org/10.1016/j.palaeo.2015.10.005

Açıkalın, S., Vellekoop, J., Ocakoğlu, F., Yılmaz, İ. Ö., Smit, J., Altıner, S. Ö., et al. (2015). Geochemical and palaeontological characterization of a new K-Pg Boundary locality from the Northern branch of the Neo-Tethys: Mudurnu – Göynük Basin, NW Turkey. *Cretaceous Research*, *52*, 251–267. https://doi.org/10.1016/j.cretres.2014.07.011

Advokaat, E. L., van Hinsbergen, D. J. J., Kaymakcı, N., Vissers, R. L. M., & Hendriks, B. W. H. (2014). Late Cretaceous extension and Palaeogene rotation-related contraction in Central Anatolia recorded in the Ayhan-Büyükkışla basin. *International Geology Review*, *56*(15), 1813–1836. https://doi.org/10.1080/00206814.2014.954279

Akbayram, K., Sengor, A. M. C., & Ozcan, E. (2016). The evolution of the intra-Pontide suture; implications of the discovery of late Cretaceous-early Tertiary melanges. In R. Sorkhabi (Ed.), *Tectonic Evolution, Collision, and Seismicity of Southwest Asia: In Honor of Manuel Berberian's Forty-Five Years of Research Contributions*, *Geological Society of America Special Publication*, (Vol. 525). https://doi.org/10.1130/2016.2525(18

Aksay, A., Pehlivan, Ş., Gedik, İ., Bılginer, E., Duru, M., Akbaş, B., & Altun, I. (2002). *Geologic map of Turkey (Zonguldak, Scale 1:500,000)*. Ankara: General Directorate of Mineral Exploration and Research (MTA).

Altiner, D., Kocyigit, A., Farinacci, A., Nicosia, U., & Conti, M. A. (1991). Jurrasic-Lower Cretaceous stratigraphy and paleogeographic evolution of the southern part of North-Western Anatolia (Turkey). *Geologica Romana*, *27*, 13–80.

Altunkaynak, Ş. (2007). Collision-driven slab breakoff magmatism in northwestern Anatolia, Turkey. *The Journal of Geology*, *115*(1), 63–82. https://doi.org/10.1086/509268

Altunkaynak, Ş., Sunal, G., Aldanmaz, E., Genç, C. Ş., Dilek, Y., Furnes, H., et al. (2012). Eocene Granitic Magmatism in NW Anatolia (Turkey) revisited: New implications from comparative zircon SHRIMP U–Pb and 40Ar–39Ar geochronology and isotope geochemistry on magma genesis and emplacement. *Lithos*, *155*, 289–309. https://doi.org/10.1016/j.lithos.2012.09.008

Black, L. P., Kamo, S. L., Allen, C. M., Davis, D. W., Aleinikoff, J. N., Valley, J. W., et al. (2004). Improved 206Pb/238U microprobe geochronology by the monitoring of a trace-element-related matrix effect; SHRIMP, ID–TIMS, ELA–ICP–MS and oxygen isotope documentation for a series of zircon standards. *Chemical Geology*, *205*(1–2), 115–140. https://doi.org/10.1016/j.chemgeo.2004.01.003

Botev, Z. I., Grotowski, J. F., & Kroese, D. P. (2010). Kernel density estimation via diffusion. *The Annals of Statistics*, *38*(5), 2916–2957. https://doi.org/10.1214/10-AOS799

Burbank, D. W., Beck, R. A., Raynolds, R. G. H., Hobbs, R., & Tahirkheli, R. A. K. (1988). Thrusting and gravel progradation in foreland basins: A test of post-thrusting gravel dispersal. *Geology*, *16*(12), 1143. https://doi.org/10.1130/0091-7613(1988)016<1143:TAGPIF>2.3.CO;2

Campbell, C. F. (2017). Tectonic evolution of the Izmir-Ankara suture zone in northwest Turkey using zircon U-Pb geochronology and zircon Lu-Hf isotopic tracers (M.S.). University of Kansas, United States. Retrieved from. http://search.proquest.com/pqdtglobal/docview/2019635859/abstract/4D50BF261D204844PQ/1

Chapman, J. B., Ducea, M. N., Kapp, P., Gehrels, G. E., & DeCelles, P. G. (2017). Spatial and temporal radiogenic isotopic trends of magmatism in Cordilleran orogens. *Gondwana Research*, *48*, 189–204. https://doi.org/10.1016/j.gr.2017.04.019

Cowie, P. A., & Scholz, C. H. (1992). Displacement-length scaling relationship for faults: Data synthesis and discussion. *Journal of Structural Geology*, *14*(10), 1149–1156. https://doi.org/10.1016/0191-8141(92)90066-6

Davies, J. H., & von Blanckenburg, F. (1995). Slab breakoff: A model of lithosphere detachment and its test in the magmatism and deformation of collisional orogens. *Earth and Planetary Science Letters*, *129*(1), 85–102. https://doi.org/10.1016/0012-821X(94)00237-S

Dickinson, W. R. (1985). Interpreting provenance relations from detrital modes of sandstones. In G. G. Zuffa (Ed.), *Provenance of Arenites*, (pp. 333–361). Dordrecht: Reidel. https://doi.org/10.1007/978-94-017-2809-6_15

Dickinson, W. R., Beard, L. S., Brakenridge, G. R., Erjavec, J. L., Ferguson, R. C., Inman, K. F., et al. (1983). Provenance of North American Phanerozoic sandstones in relation to tectonic setting. *Geological Society of America Bulletin*, *94*(2), 222. https://doi.org/10.1130/0016-7606(1983)94<222:PONAPS>2.0.CO;2

Dickinson, W. R., Klute, M. A., Hayes, M. J., Janecke, S. U., Lundin, E. R., McKITTRICK, M. A., & Olivares, M. D. (1988). Paleogeographic and paleotectonic setting of Laramide sedimentary basins in the central Rocky Mountain region. *GSA Bulletin*, *100*(7), 1023–1039. https://doi.org/10.1130/0016-7606(1988)100<1023:PAPSOL>2.3.CO;2

Dickinson, W. R., & Suczek, C. A. (1979). Plate tectonics and sandstone compositions. *AAPG Bulletin*, *63*(12), 2164–2182.

Dilek, Y., & Altunkaynak, Ş. (2009). Geochemical and temporal evolution of Cenozoic magmatism in western Turkey: Mantle response to collision, slab break-off, and lithospheric tearing in an orogenic belt. *Geological Society, London, Special Publications*, *311*(1), 213–233. https://doi.org/10.1144/SP311.8

Duru, M., & Aksay, A. (2002). *Geologic map of the Adapazarı quadrangle (Sheet H 24, Scale 1:100,000)*. Ankara: General Directorate of Mineral Exploration and Research (MTA).

Eddy, M. P., Bowring, S. A., Miller, R. B., & Tepper, J. H. (2016). Rapid assembly and crystallization of a fossil large-volume silicic magma chamber. *Geology*, *44*(4), 331–334. https://doi.org/10.1130/G37631.1

Ersoy, E. Y., Akal, C., Genç, Ş. C., Candan, O., Palmer, M. R., Prelević, D., et al. (2017). U-Pb zircon geochronology of the Paleogene-Neogene volcanism in the NW Anatolia: Its implications for the Late Mesozoic-Cenozoic geodynamic evolution of the Aegean. *Tectonophysics*, *717*, 284–301. https://doi.org/10.1016/j.tecto.2017.08.016

Ersoy, E. Y., Palmer, M. R., Genç, Ş. C., Prelević, D., Akal, C., & Uysal, İ. (2017). Chemo-probe into the mantle origin of the NW Anatolia Eocene to Miocene volcanic rocks: Implications for the role of, crustal accretion, subduction, slab roll-back and slab break-off processes in genesis of post-collisional magmatism. *Lithos*, *288-289*, 55–71. https://doi.org/10.1016/j.lithos.2017.07.006

Flemings, P. B., & Jordan, T. E. (1990). Stratigraphic modeling of foreland basins: Interpreting thrust deformation and lithosphere rheology. *Geology*, *18*(5), 430–434. https://doi.org/10.1130/0091-7613(1990)018<0430:SMOFBI>2.3.CO;2

Floyd, P. A., Göncüoğlu, M. C., Winchester, J. A., & Yaliniz, M. K. (2000). Geochemical character and tectonic environment of Neotethyan ophiolitic fragments and metabasites in the Central Anatolian Crystalline Complex, Turkey. *Geological Society, London, Special Publications*, *173*(1), 183–202. https://doi.org/10.1144/GSL.SP.2000.173.01.09

Garzanti, E. (2018). Petrographic classification of sand and sandstone. *Earth-Science Reviews*, *192*, 545–563. https://doi.org/10.1016/j.earscirev.2018.12.014

Garzanti, E., Radeff, G., & Malusà, M. G. (2018). Slab breakoff: A critical appraisal of a geological theory as applied in space and time. *Earth-Science Reviews*, *177*, 303–319. https://doi.org/10.1016/j.earscirev.2017.11.012

Gedik, İ., & Aksay, A. (2002). *Geologic map of the Adapazarı quadrangle (Sheet H 25, Scale 1:100,000)*. Ankara: General Directorate of Mineral Exploration and Research (MTA).

Gehrels, G. (2012). Detrital zircon U-Pb geochronology: Current methods and new opportunities. In C. Busby, & A. Azor (Eds.), *Tectonics of Sedimentary Basins*, (pp. 45–62). Chichester, UK: John Wiley & Sons, Ltd. https://doi.org/10.1002/9781444347166.ch2

Gehrels, G. (2014). Detrital zircon U-Pb geochronology applied to tectonics. *Annual Review of Earth and Planetary Sciences*, *42*(1), 127–149. https://doi.org/10.1146/annurev-earth-050212-124012

Göncüoğlu, M. C., Turhan, N., Şentürk, K., Özcan, A., Uysal, Ş., & Yaliniz, M. K. (2000). A geotraverse across northwestern Turkey: Tectonic units of the Central Sakarya region and their tectonic evolution. *Geological Society, London, Special Publications*, *173*(1), 139–161. https://doi.org/10.1144/GSL.SP.2000.173.01.06

Görür, N., Oktay, F. Y., Seymen, I., & Şengör, A. M. C. (1984). Palaeotectonic evolution of the Tuzgölü basin complex, Central Turkey: Sedimentary record of a Neo-Tethyan closure. *Geological Society, London, Special Publications*, *17*(1), 467–482. https://doi.org/10.1144/GSL.SP.1984.017.01.34

Görür, N., Tüysüz, O., & Celal Şengör, A. M. (1998). Tectonic evolution of the central Anatolian basins. *International Geology Review*, *40*(9), 831–850. https://doi.org/10.1080/00206819809465241

Graham, D. J., & Midgley, N. G. (2000). Graphical representation of particle shape using triangular diagrams: An Excel spreadsheet method. *Earth Surface Processes and Landforms*, *25*(13), 1473–1477. https://doi.org/10.1002/1096-9837(200012)25:13<1473::AID-ESP158>3.0.CO;2-C

Gürer, D., & van Hinsbergen, D. J. J. (2018). Diachronous demise of the Neotethys Ocean as a driver for non-cylindrical orogenesis in Anatolia. *Tectonophysics*, *760*, 95–106. https://doi.org/10.1016/j.tecto.2018.06.005

Gürer, D., van Hinsbergen, D. J. J., Matenco, L., Corfu, F., & Cascella, A. (2016). Kinematics of a former oceanic plate of the Neotethys revealed by deformation in the Ulukışla basin (Turkey): Kinematic evolution of central Anatolia. *Tectonics*, *35*, 2385–2416. https://doi.org/10.1002/2016TC004206

Harris, N. B. W., Kelley, S., & Okay, A. I. (1994). Post-collisional magmatism and tectonics in northwest Anatolia. *Contributions to Mineralogy and Petrology*, *117*(3), 241–252. https://doi.org/10.1007/BF00310866

Heller, P. L., & Paola, C. (1992). The large-scale dynamics of grain-size variation in alluvial basins, 2: Applications to syntectonic conglomerate. *Basin Research*, *4*(2), 91–102. https://doi.org/10.1111/j.1365-2117.1992.tb00146.x

Hippolyte, J.-C., Espurt, N., Kaymakci, N., Sangu, E., & Müller, C. (2016). Cross-sectional anatomy and geodynamic evolution of the Central Pontide orogenic belt (northern Turkey). *International Journal of Earth Sciences*, *105*(1), 81–106. https://doi.org/10.1007/s00531-015-1170-6

Janbu, N. E., Nemec, W., Kirman, E., & zaksoy, V. (2007). Facies anatomy of a sand-rich channelized turbiditic system: The Eocene Kusuri Formation in the Sinop Basin, north-central Turkey. In G. Nichols, E. Williams, & C. Paola (Eds.), *Sedimentary Processes, Environments and Basins*, (pp. 457–517). Oxford, UK: Blackwell Publishing Ltd. https://doi.org/10.1002/9781444304411.ch19

Jones, M. F., Coster, P. M. C., Licht, A., Métais, G., Ocakoğlu, F., Taylor, M. H., & Beard, K. C. (2018). A stem bat (Chiroptera: Palaeochiropterygidae) from the late middle Eocene of northern Anatolia: Implications for the dispersal and palaeobiology of early bats. *Palaeobiodiversity and Palaeoenvironments*, *99*(2), 261–269. https://doi.org/10.1007/s12549-018-0338-z

Kasapoğlu, B., Ersoy, Y. E., Uysal, İ., Palmer, M. R., Zack, T., Koralay, E. O., & Karlsson, A. (2016). The petrology of Paleogene volcanism in the Central Sakarya, Nallıhan Region: Implications for the initiation and evolution of post-collisional, slab break-off-related magmatic activity. *Lithos*, *246-247*, 81–98. https://doi.org/10.1016/j.lithos.2015.12.024

Kaymakci, N., Özçelik, Y., White, S. H., & Van Dijk, P. M. (2009). Tectono-stratigraphy of the Çankırı Basin: Late Cretaceous to early Miocene evolution of the Neotethyan Suture Zone in Turkey. *Geological Society, London, Special Publications*, *311*(1), 67–106. https://doi.org/10.1144/SP311.3

Kaymakci, N., White, S. H., & Vandijk, P. M. (2003). Kinematic and structural development of the Çankiri Basin (Central Anatolia, Turkey): A paleostress inversion study. *Tectonophysics*, *364*(1–2), 85–113. https://doi.org/10.1016/S0040-1951(03)00043-X

Kibici, Y., İlbeyli, N., Yıldız, A., & Bağcı, M. (2010). Geochemical constraints on the genesis of the Sarıcakaya intrusive rocks, Turkey: Late Paleozoic crustal melting in the central Sakarya Zone. *Chemie der Erde*, *70*(3), 243–256. https://doi.org/10.1016/j.chemer.2009.12.001

Lefebvre, C., Meijers, M. J. M., Kaymakci, N., Peynircioğlu, A., Langereis, C. G., & van Hinsbergen, D. J. J. (2013). Reconstructing the geometry of central Anatolia during the late Cretaceous: Large-scale Cenozoic rotations and deformation between the Pontides and Taurides. *Earth and Planetary Science Letters*, *366*, 83–98. https://doi.org/10.1016/j.epsl.2013.01.003

Leren, B. L. S., Janbu, N. E., Nemec, W., Kirman, E., & Ilgar, A. (2007). Late Cretaceous to Early Eocene sedimentation in the Sinop–Boyabat Basin, north-central Turkey: A deep-water turbiditic system evolving into littoral carbonate platform. In G. Nichols, E. Williams, & C. Paola (Eds.), *Sedimentary Processes, Environments and Basins*, (pp. 401–456). Oxford, UK: Blackwell Publishing Ltd. https://doi.org/10.1002/9781444304411.ch18

Licht, A., Coster, P., Ocakoğlu, F., Campbell, C., Métais, G., Mulch, A., et al. (2017). Tectono-stratigraphy of the Orhaniye Basin, Turkey: Implications for collision chronology and Paleogene biogeography of central Anatolia. *Journal of Asian Earth Sciences*, *143*, 45–58. https://doi.org/10.1016/j.jseaes.2017.03.033

Licht, A., Dupont-Nivet, G., Win, Z., Swe, H. H., Kaythi, M., Roperch, P., et al. (2018). Paleogene evolution of the Burmese forearc basin and implications for the history of India-Asia convergence. *GSA Bulletin*, *131*(5-6), 730–748. https://doi.org/10.1130/B35002.1

Ludwig, K. R. (2012). *User's Manual for Isoplot 3.75: A Geochronological Toolkit for Microsoft Excel*, *Berkeley Geochronological Center*, (pp. 1–75). Berkeley, CA: Special Publication No. 5

Marrett, R., & Allmendinger, R. W. (1991). Estimates of strain due to brittle faulting: sampling of fault populations. *Journal of Structural Geology*, *13*(6), 735–738. https://doi.org/10.1016/0191-8141(91)90034-G

Meijers, M. J. M., Kaymakci, N., van Hinsbergen, D. J. J., Langereis, C. G., Stephenson, R. A., & Hippolyte, J.-C. (2010). Late Cretaceous to Paleocene oroclinal bending in the central Pontides (Turkey). *Tectonics*, *29*, TC4016. https://doi.org/10.1029/2009TC002620

Menant, A., Jolivet, L., & Vrielynck, B. (2016). Kinematic reconstructions and magmatic evolution illuminating crustal and mantle dynamics of the eastern Mediterranean region since the late Cretaceous. *Tectonophysics*, *675*, 103–140. https://doi.org/10.1016/j.tecto.2016.03.007

Métais, G., Beard, K., Erdal, O., & Erturaç, K. (2017). Tarsal morphology of the pleuraspidotheriid mammal Hilalia from the middle Eocene of Turkey. *Acta Palaeontologica Polonica*, *62*. https://doi.org/10.4202/app.00314.2016

Métais, G., Coster, P. M., Kappelman, J. R., Licht, A., Ocakoglu, F., Taylor, M. H., & Beard, K. C. (2018). Eocene metatherians from Anatolia illuminate the assembly of an island fauna during Deep Time. *PLoS ONE*, *13*(11), e0206181. https://doi.org/10.1371/journal.pone.0206181

Nairn, S. P., Robertson, A. H. F., Ünlügenç, U. C., Tasli, K., & İnan, N. (2013). Tectonostratigraphic evolution of the Upper Cretaceous–Cenozoic central Anatolian basins: An integrated study of diachronous ocean basin closure and continental collision. *Geological Society, London, Special Publications*, *372*(1), 343–384. https://doi.org/10.1144/SP372.9

Nichols, G. (2009). *Sedimentology and stratigraphy*, (2nd ed.pp. 129–161). Chichester, UK; Hoboken, NJ: Wiley-Blackwell.

Niu, Y. (2017). Slab breakoff: A causal mechanism or pure convenience? *Science Bulletin*, *62*(7), 456–461. https://doi.org/10.1016/j.scib.2017.03.015

Noda, A. (2016). Forearc basins: Types, geometries, and relationships to subduction zone dynamics. *Geological Society of America Bulletin*, *128*(5–6), 879–895. https://doi.org/10.1130/B31345.1

Ocakoğlu, F., Açıkalın, S., Yılmaz, I. ö., Şafak, ü., & Gökçeoğlu, C. (2012). Evidence of orbital forcing in lake-level fluctuations in the Middle Eocene oil shale-bearing lacustrine successions in the Mudurnu-Göynük Basin, NW Anatolia (Turkey). *Journal of Asian Earth Sciences*, *56*, 54–71. https://doi.org/10.1016/j.jseaes.2012.04.021

Ocakoğlu, F., Hakyemez, A., Açıkalın, S., Özkan Altıner, S., Büyükmeriç, Y., Licht, A., et al. (2018). Chronology of subduction and collision along the İzmir-Ankara suture in Western Anatolia: Records from the Central Sakarya Basin. *International Geology Review*, *61*(10), 1244–1269. https://doi.org/10.1080/00206814.2018.1507009

Okay, A., & Satir, M. (2006). Geochronology of Eocene plutonism and metamorphism in northwest. *Geodinamica Acta*, *19*(5), 251–266. https://doi.org/10.3166/ga.19.251-266

Okay, A. İ. (2000). Was the Late Triassic orogeny in Turkey caused by the collision of an oceanic plateau? *Geological Society, London, Special Publications*, *173*(1), 25–41. https://doi.org/10.1144/GSL.SP.2000.173.01.02

Okay, A. I. (2002). Jadeite-chloritoid-glaucophane-lawsonite blueschists in north-west Turkey: Unusually high P/T ratios in continental crust: jadeite-chloritoid-lawsonite blueschists. *Journal of Metamorphic Geology*, *20*(8), 757–768. https://doi.org/10.1046/j.1525-1314.2002.00402.x

Okay, A. I., & Göncüoglu, M. C. (2004). The Karakaya Complex: A review of data and concepts. *Turkish Journal of Earth Sciences*, *13*(2), 77–95.

Okay, A. I., Harris, N. B. W., & Kelley, S. P. (1998). Exhumation of blueschists along a Tethyan suture in northwest Turkey. *Tectonophysics*, *285*(3–4), 275–299. https://doi.org/10.1016/S0040-1951(97)00275-8

Okay, A. I., Monod, O., & Monié, P. (2002). Triassic blueschists and eclogites from northwest Turkey: Vestiges of the Paleo-Tethyan subduction. *Lithos*, *64*(3), 155–178. https://doi.org/10.1016/S0024-4937(02)00200-1

Okay, A. I., Tansel, I., & Tüysüz, O. (2001). Obduction, subduction and collision as reflected in the Upper Cretaceous-Lower Eocene sedimentary record of western Turkey. *Geological Magazine*, *138*(2), 117–142. https://doi.org/10.1017/S0016756801005088

Okay, A. I., & Whitney, D. L. (2010). Blueschists, eclogites, ophiolites and suture zones in northwest turkey: A review and a field excursion guide. *Ofioliti*, *35*(2), 131–172.

Özdamar, Ş., Sunal, G., Demiroğlu, M., Yaltirak, C., Billor, M. Z., Georgiev, S., et al. (2018). Metamorphism, magmatism, and exhumation history of the Tavşanlı Zone, NW Turkey: New petrological constraints. *Turkish Journal of Earth Sciences*, *27*(4), 269–293. https://doi.org/10.3906/yer-1712-14

Paola, C., Heller, P. L., & Angevine, C. L. (1992). The large-scale dynamics of grain-size variation in alluvial basins, 1: Theory. *Basin Research*, *4*(2), 73–90. https://doi.org/10.1111/j.1365-2117.1992.tb00145.x

Paton, C., Hellstrom, J., Paul, B., Woodhead, J., & Hergt, J. (2011). Iolite: Freeware for the visualisation and processing of mass spectrometric data. *Journal of Analytical Atomic Spectrometry*, *26*(12), 2508. https://doi.org/10.1039/c1ja10172b

Plunder, A., Agard, P., Chopin, C., & Okay, A. I. (2013). Geodynamics of the Tavşanlı zone, western Turkey: Insights into subduction/obduction processes. *Tectonophysics*, *608*, 884–903. https://doi.org/10.1016/j.tecto.2013.07.028

Plunder, A., Plunder, A., Thieulot, C., & Hinsbergen, D. J. J. v. (2018). The effect of obliquity on temperature in subduction zones: Insights from 3-D numerical modeling. *Solid Earth*, *9*(3), 759–776. https://doi.org/10.5194/se-9-759-2018

Portner, D. E., Delph, J. R., Biryol, C. B., Beck, S. L., Zandt, G., Özacar, A. A., et al. (2018). Subduction termination through progressive slab deformation across Eastern Mediterranean subduction zones from updated *P*-wave tomography beneath Anatolia. *Geosphere*, *14*(3), 907–925. https://doi.org/10.1130/GES01617.1

Pourteau, A., Candan, O., & Oberhänsli, R. (2010). High-pressure metasediments in central Turkey: Constraints on the Neotethyan closure history. *Tectonics*, *29*, TC5004. https://doi.org/10.1029/2009TC002650

Pourteau, A., Oberhänsli, R., Candan, O., Barrier, E., & Vrielynck, B. (2016). Neotethyan closure history of western Anatolia: A geodynamic discussion. *International Journal of Earth Sciences*, *105*(1), 203–224. https://doi.org/10.1007/s00531-015-1226-7

Pourteau, A., Sudo, M., Candan, O., Lanari, P., Vidal, O., & Oberhänsli, R. (2013). Neotethys closure history of Anatolia: insights from ^{40}Ar-^{39}Ar geochronology and *P-T* estimation in high-pressure metasedimentary rocks. *Journal of Metamorphic Geology*, *31*(6), 585–606. https://doi.org/10.1111/jmg.12034

Prothero, D. R., & Schwab, F. (1996). *Sedimentary geology: An introduction to sedimentary rocks and stratigraphy*, (pp. 67–167). New York: W. H. Freeman.

Retallack, G. J. (1988). Field recognition of paleosols. *Special Paper of the Geological Society of America*, *216*, 1–20. https://doi.org/10.1130/SPE216-p1

Robertson, A. H. F., Parlak, O., & Ustaömer, T. (2009). Melange genesis and ophiolite emplacement related to subduction of the northern margin of the Tauride–Anatolide continent, central and western Turkey. *Geological Society, London, Special Publications*, *311*(1), 9–66. https://doi.org/10.1144/SP311.2

Robertson, A. H. F., & Ustaömer, T. (2004). Tectonic evolution of the Intra-Pontide suture zone in the Armutlu Peninsula, NW Turkey. *Tectonophysics*, *381*(1–4), 175–209. https://doi.org/10.1016/j.tecto.2002.06.002

Şahin, M., Yaltırak, C., & Karacık, Z. (2019). A case study of compression to escape tectonic transition: Tectonic evolution of the Nallıhan Wedge and comparison with the Tercan Wedge (Eastern Mediterranean, Turkey). *Journal of Asian Earth Sciences*, *174*, 311–331. https://doi.org/10.1016/j.jseaes.2018.12.016

Sarıfakıoğlu, E., Dilek, Y., & Sevin, M. (2017). New synthesis of the İzmir-Ankara-Erzincan suture zone and the Ankara mélange in northern Anatolia based on new geochemical and geochronological constraints. In R. Sorkhabi (Ed.), *Tectonic Evolution, Collision, and Seismicity of Southwest Asia: In Honor of Manuel Berberian's Forty-Five Years of Research Contributions*, Geological Society of America Special Paper 525, (pp. 1–63)

Schleiffarth, W. K., Darin, M. H., Reid, M. R., & Umhoefer, P. J. (2018). Dynamics of episodic Late Cretaceous-Cenozoic magmatism across Central to Eastern Anatolia: New insights from an extensive geochronology compilation. *Geosphere*, *14*(5), 1990–2008. https://doi.org/10.1130/GES01647.1

Sen, S. (2013). Dispersal of African mammals in Eurasia during the Cenozoic: Ways and whys. *Geobios*, *46*(1–2), 159–172. https://doi.org/10.1016/j.geobios.2012.10.012

Şengör, A. M. C. (1979). Mid-Mesozoic closure of Permo-Triassic Tethys and its implications. *Nature*, *279*(5714), 590–593. https://doi.org/10.1038/279590a0

Şengör, A. M. C., & Yilmaz, Y. (1981). Tethyan evolution of turkey: A plate tectonic approach. *Tectonophysics*, *75*(3-4), 181–241. https://doi.org/10.1016/0040-1951(81)90275-4

Şengüler, İ., & Izladi, E. (2013). Neogene stratigraphy of the Eskişehir Graben and the investigation of coal deposition by seismic reflection method. *Bulletin of MTA*, *146*, 105–116.

Sherlock, S., Kelley, S., Inger, S., Harris, N., & Okay, A. (1999). ^{40}Ar-^{39}Ar and Rb-Sr geochronology of high-pressure metamorphism and exhumation history of the Tavsanli Zone, NW Turkey. *Contributions to Mineralogy and Petrology*, *137*(1–2), 46–58. https://doi.org/10.1007/PL00013777

Sláma, J., Košler, J., Condon, D. J., Crowley, J. L., Gerdes, A., Hanchar, J. M., et al. (2008). Plešovice zircon—A new natural reference material for U-Pb and Hf isotopic microanalysis. *Chemical Geology*, *249*(1-2), 1–35. https://doi.org/10.1016/j.chemgeo.2007.11.005

Timur, E., & Aksay, A. (2002). *Geologic map of the Adapazarı quadrangle (Sheet H 26, Scale 1:100,000)*. Ankara: General Directorate of Mineral Exploration and Research (MTA).

Turhan, N. (2002). *Geologic map of Turkey (Ankara, Scale 1:500,000)*. Ankara: General Directorate of Mineral Exploration and Research (MTA).

Uğuz, M. F. (2013). A new age finding in the Central Sakarya Region (NW Turkey). *Bulletin of MTA*, *146*, 1–25.

Ustaömer, P. A., Ustaömer, T., Collins, A. S., & Reischpeitsch, J. (2009). Lutetian arc-type magmatism along the southern Eurasian margin: New U-Pb LA-ICPMS and whole-rock geochemical data from Marmara Island, NW Turkey. *Mineralogy and Petrology*, *96*(3-4), 177–196. https://doi.org/10.1007/s00710-009-0051-8

Ustaömer, P. A., Ustaömer, T., & Robertson, A. H. F. (2012). Ion probe U-Pb dating of the Central Sakarya basement: A peri-Gondwana terrane intruded by late Lower Carboniferous subduction/collision-related granitic rocks. *Turkish Journal of Earth Sciences*, *21*(6), 905–932. https://doi.org/10.3906/yer-1103-1

Ustaömer, T., Ustaömer, P. A., Robertson, A. H. F., & Gerdes, A. (2016). Implications of U-Pb and Lu-Hf isotopic analysis of detrital zircons for the depositional age, provenance and tectonic setting of the Permian-Triassic Palaeotethyan Karakaya Complex, NW Turkey. *International Journal of Earth Sciences*, *105*(1), 7–38. https://doi.org/10.1007/s00531-015-1225-8

van Hinsbergen, D. J. J., Kaymakci, N., Spakman, W., & Torsvik, T. H. (2010). Reconciling the geological history of western Turkey with plate circuits and mantle tomography. *Earth and Planetary Science Letters*, *297*(3–4), 674–686. https://doi.org/10.1016/j.epsl.2010.07.024

van Hinsbergen, D. J. J., Maffione, M., Plunder, A., Kaymakcı, N., Ganerød, M., Hendriks, B. W. H., et al. (2016). Tectonic evolution and paleogeography of the Kırşehir Block and the Central Anatolian Ophiolites, Turkey. *Tectonics*, *35*, 983–1014. https://doi.org/10.1002/2015TC004018

Vermeesch, P. (2013). Multi-sample comparison of detrital age distributions. *Chemical Geology*, *341*, 140–146. https://doi.org/10.1016/j.chemgeo.2013.01.010

Vermeesch, P. (2018). IsoplotR: A free and open toolbox for geochronology. *Geoscience Frontiers*, *9*(5), 1479–1493. https://doi.org/10.1016/j.gsf.2018.04.001

von Blanckenburg, F., & Davies, J. H. (1995). Slab breakoff: A model for syncollisional magmatism and tectonics in the Alps. *Tectonics*, *14*(1), 120–131. https://doi.org/10.1029/94TC02051

Walsh, J. J., & Watterson, J. (1988). Analysis of the relationship between displacements and dimensions of faults. *Journal of Structural Geology*, *10*(3), 239–247. https://doi.org/10.1016/0191-8141(88)90057-0

Yaliniz, M. K., Göncüoğlu, M. C., & Ozkan-Altiner, S. (2000). Formation and emplacement ages of the SSZ-type Neotethyan ophiolites in Central Anatolia, Turkey: Palaeotectonic implications. *Geological Journal*, *35*(2), 53–68. https://doi.org/10.1002/1099-1034(200004/06)35:2<53::AID-GJ837>3.0.CO;2-6

Yildiz, A., Kibici, Y., Bağci, M., Dumlupunar, İ., Kocabaş, C., & Aritan, A. E. (2015). Petrogenesis of the post-collisional Eocene volcanic rocks from the Central Sakarya Zone (Northwestern Anatolia, Turkey): Implications for source characteristics, magma evolution, and tectonic setting. *Arabian Journal of Geosciences*, *8*(12), 11239–11260. https://doi.org/10.1007/s12517-015-1991-4